ACS Catalysis

pubs.acs.org/acscatalysis

Research Article

# Impact of Metal and Heteroatom Identities in the Hydrogenolysis of C−X Bonds (X = C, N, O, S, and Cl)

Abdulrahman S. Almithn and David D. Hibbitts*

Cite This: *ACS Catal.* 2020, 10, 5086−5100

Read Online

ACCESS | Metrics & More | Article Recommendations | Supporting Information

**ABSTRACT:** Hydrogenolysis of complex heteroatom-containing organic molecules plays a large role in upgrading fossil- and biomass-based fuel and chemical feedstocks, such as hydrodeoxygenation and desulfurization. Here, we present a fundamental study contrasting the cleavage of C−X bonds in ethane, methylamine, methanol, methanethiol, and chloromethane on group 8−11 transition metals (Ru, Os, Co, Rh, Ir, Ni, Pd, Pt, Cu, Ag, and Au) using density functional theory (DFT). Previous kinetic and DFT studies have shown that hydrogenolysis of unsubstituted C−C bonds in alkanes occur via unsaturated intermediates (e.g., *CHCH* for ethane) after a series of quasi-equilibrated dehydrogenation steps that weaken the C−C bond by creating C−metal bonds. However, the effects of the substituent group in $CH_3XH_n$ on the required degree of unsaturation to cleave the C−X have not been systematically studied and are critical to understanding heteroatom removal. DFT-predicted free energy barriers indicate that the carbon atom in C−X generally cleaves after the removal of 2 H atoms (to form CH*) on group 8−10 metals regardless of the identity of the metal or the heteroatom. Group 11 metals (coinage metals: Cu, Ag, and Au) generally cleave the C−X bond in the most H-saturated intermediates with barriers close to thermal activation of C−X in gaseous $CH_3XH_n$ molecules. The N-leaving group in C−N cleavage depends on the metal identity as it can leave fully dehydrogenated (as N*) on group 8 metals and partially or fully hydrogenated (as NH* or $NH_2$*) on group 9−11 metals. Although O and S are both group 16 elements, C−S bonds always cleave to form S* (losing one H), while C−O bonds generally cleave to form OH* (without preceding H removal). Cl does not have H atoms to be removed before C−Cl cleavage in $CH_3Cl$, and thus the C atom sacrifices an additional H atom to weaken the C−Cl bond on group 8 metals. This study of heteroatom removal from simple organic molecules is the first step to providing fundamental insights into $H_2$-based upgrading of more complex organic molecules.

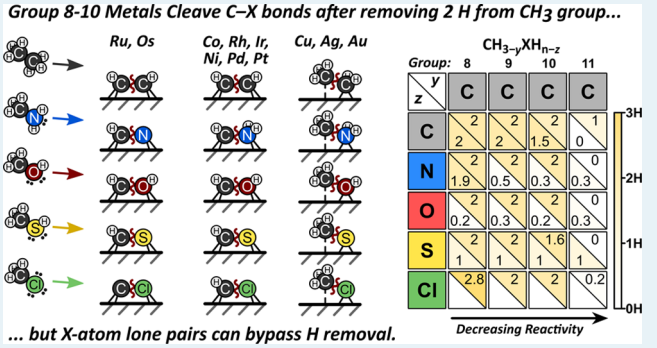


**KEYWORDS:** *hydrogenolysis, denitrogenation, deoxygenation, dechlorination, metal catalysis*



## 1. INTRODUCTION

Using $H_2$ to cleave chemical bonds (hydrogenolysis) is a critical reaction in the areas of petroleum refining (where metal-catalyzed C−C cleavage is undesired and C−N and C−S cleavages are desired), biomass upgrading to fuels or chemical (desired complete or selective C−O cleavage), and wastewater upgrading (desired C−Cl cleavage).[1−4] Bond dissociation energies (BDEs) for these gas-phase molecules[5−8] can give some insights into reactivity. However, in practical applications, we must understand how these chemical bonds are weakened by interactions with catalytic surfaces, such as transition-metal surfaces, upon different extents of dehydrogenation to optimally design and operate chemical processes. Studying the effects of the substituent group, the degree of unsaturation, and the catalyst identity on weakening and cleaving the C−X bond (X = C, N, O, S, and Cl) can provide fundamental insights for related chemistry such as alkane hydrogenolysis,[9−14] hydrodenitrogenation,[15−18] deoxygenation,[19−23] desulfurization,[24−27] and dechlorination.[1−4]

Previous high-pressure kinetic and density functional theory (DFT) studies demonstrated that C−C bond cleavage in ethane occurs via *CHCH* intermediates, which have lost 4 H atoms through quasi-equilibrated dehydrogenation steps prior to C−C bond activation on Ir catalysts;[9,14,28] C−H bonds are replaced with C−metal bonds (C−M), which weakens the C−C bond prior to cleavage. The removed H atoms from alkanes then form $H_2$(g) molecules that increase the activation entropy and, consequently, lower the activation free energy. In our

Received: January 29, 2020
Revised: March 18, 2020
Published: April 3, 2020




https://dx.doi.org/10.1021/acscatal.0c00481
*ACS Catal.* 2020, 10, 5086−5100

recent study,[29] we demonstrated that ethane hydrogenolysis occurs via the same mechanism (via *CHCH* intermediates) over group 8−10 metals (Ru, Os, Rh, Ir, Ni, Pd, and Pt, historically known as platinum-group metals) but with catalyst activity that decreases from left to right in the periodic table. Group 11 metals Cu, Ag, and Au (historically known as coinage metals), however, favor cleaving the C−C bond in the most saturated intermediate (*$CH_3CH_2$*) with barriers approaching those of thermal activation of $CH_3CH_3$ because those metals form considerably weaker C−M bonds than group 8−10 metals, thus disfavoring the exchange of C−H bonds with C−M bonds.

Prior kinetic and DFT studies indicate that $^1$C−$^2$C and $^2$C−$^2$C bonds in larger alkanes (linear or branched, cyclic or acyclic) also cleave via *RCCR* intermediates,[9−14] whereas cleaving $^3$C−$^x$C in branched alkanes requires the removal of H atoms from other carbon atoms not involved in $^3$C−$^x$C.[10,11,13] Taken together, these findings suggest that primary ($^1$C) and secondary ($^2$C) carbon atoms always form alkylidyne species (CH* and $C_nH_{2n+1}C$*) upon C−C bond cleavage in alkanes over group 8−10 metals, regardless of the degree of substitution at the other C atom or the metal identity. C−C cleavage in butanol and propanol was examined using a combination of measured kinetics and DFT on Ir and Cu surfaces, and that work indicated that C−C bonds away from O atoms cleave in a manner identical to C−C bond cleavage in alkanes, while C−CO cleavage (decarbonylation) occurred at much higher rates, and the rate of C−O cleavage relative to the rate of decarbonylation was high on Cu and very low on Ir.[30] The role of a heteroatom (e.g., N, O) on the rate and manner of C-atom activation has not been systematically contrasted to C−C hydrogenolysis across a wide range of metals.

C−N hydrogenolysis in methylamine ($CH_3NH_2$) has been studied on various supported metal catalysts.[31−34] These studies showed that C−N hydrogenolysis in methylamine also proceeds through partially dehydrogenated surface intermediates and suggested that C−N bond cleavage is the rate-determining step on all examined metals (Re, Ru, Os, Rh, Ir, Pd, Pt, and Au). The reactivity of these metals follows a similar trend as in C−C hydrogenolysis, which decreases as one proceeds from group 7 to 10 in the periodic table. However, the identity of the hydrogen-deficient intermediate that undergoes C−N bond cleavage remains unclear. Dehydration, decarbonylation, and C−O hydrogenolysis of oxygenated hydrocarbons have been extensively studied as routes for catalytic deoxygenation to convert biomass-derived feedstock into more valuable chemicals.[30,35−38] Previous DFT studies have shown that C−O bond cleavage in ethanol and propanol occurs through *RCOH* intermediates on transition-metal surfaces.[30,36] C−S hydrogenolysis and desulfurization also play an important role in petroleum-refining processes,[39−44] while dechlorination is widely used for safe conversion of chlorinated wastes.[45−48] The C−S bond in methanethiol, for example, can be cleaved in either *$CH_3S$* or *CHS* intermediates depending on reaction conditions over Pt.[44] Despite these extensive studies, no consensus has been reached regarding the degree of unsaturation required to weaken the C−X bond being cleaved, and periodic trends in C−X bond cleavage on various metal surfaces have not been systematically addressed. The fundamental nature of these reactions has been difficult to understand, in part, because they often operate at conditions of high coverage of one or more intermediates (i.e., H*, NH*, CO*, O*, S*, Cl*), which may have severe impacts on rates and selectivities when studied experimentally. Prior to considering these coverage effects, the nearly bare reactivity must be understood and can give insights into the reaction mechanism, as shown previously for ethane hydrogenolysis on Ir and other metals.[14,28,29]

Here, we contrast activation of saturated C−X species by examining C−C bond cleavage in ethane ($CH_3CH_3$), C−N in methylamine ($CH_3NH_2$), C−O in methanol ($CH_3OH$), C−S in methanethiol ($CH_3SH$), and C−Cl in chloromethane ($CH_3Cl$) on group 8−11 transition metals to understand how C−X bonds cleave on metal surfaces, specifically, the degree of unsaturation required for the carbon atom and for the heteroatom to cleave the C−X bond. These heteroatoms cover groups 14−17 of the periodic table, with O and S in group 16, to examine the effects of heteroatom size and row in the periodic table. Through contrast with C−C hydrogenolysis in ethane, we demonstrate the influence of the heteroatom on the preferred H-content of the carbon atom and how the H-content of the heteroatom varies across the periodic table. We show that the carbon atom preferentially forms CH* upon C−X cleavage on group 8−10 metals, while group 11 metals cleave the C−X bond in $CH_3XH_n$ intermediates, consistent with C−C bond hydrogenolysis in alkanes. However, the preferred H-content on the heteroatom to cleave the C−X bond varies across the periodic table because of the presence of lone pairs on these heteroatoms. Such universal preference for the carbon atom to form CH*-containing intermediates upon cleavage regardless of the identity of the heteroatom provides a key mechanistic "rule" that is applicable to hydrotreating a wide range of reactants.

## 2. COMPUTATIONAL METHODS

Periodic planewave density functional theory (DFT) calculations were performed using the Vienna ab initio simulation package (VASP)[49−52] as implemented in the computational catalysis interface (CCI).[53] Planewaves were constructed using projector augmented-wave (PAW) potentials with an energy cutoff of 396 eV.[54,55] The revised Perdew−Burke−Ernzerhof (RPBE) form of the generalized gradient approximation (GGA) was used to describe exchange and correlation energies.[56−58] Wave functions were converged until electronic energies varied less than $10^{-6}$ eV. Forces on all atoms were determined using a fast Fourier transform (FFT) grid with a cutoff equal to twice the planewave cutoff, and structures were geometrically optimized until the forces on all atoms were less than 0.05 eV Å$^{-1}$. Gas-phase calculations were modeled within an 18 × 18 × 18 Å$^3$ unit cell of empty space, and the Brillouin zone for such calculations was sampled at the Γ-point. Gas-phase bond dissociation energies were calculated by computing the spin-polarized potential energies for the radical fragments formed via C−X dissociation in fully saturated $CH_3XH_n$ intermediates.

Close-packed metal surfaces—(111) surfaces for face-centered cubic (FCC) metals and (001) surfaces for HCP metals—were modeled as 3 × 3 periodic lattices with four layers orthogonal to the surface and 10 Å of vacuum separating slabs; the bottom two layers were fixed in their bulk positions, and the top two layers were relaxed. A 4 × 4 × 1 Monkhorst−Pack sampling of the first Brillouin zone ($k$-point mesh)[59,60] was used during a two-step geometric convergence that initially converges structures (to a force of 0.05 eV Å$^{-1}$) with wave functions converged to $10^{-4}$ eV and an FFT grid 1.5× the planewave cutoff. The second step then reoptimizes that


https://dx.doi.org/10.1021/acscatal.0c00481
ACS Catal. 2020, 10, 5086−5100

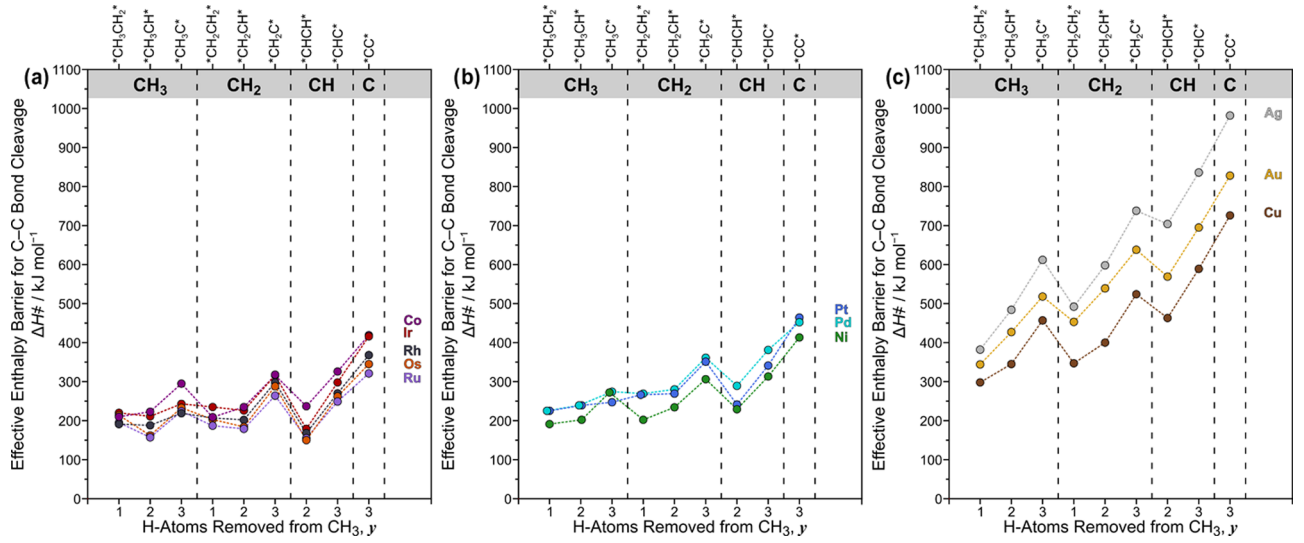


**Figure 1.** Effective enthalpy barriers ($\Delta H^{\ddagger}$; eq 1) for C−C bond cleavage in ethane-derived intermediates on (a) groups 8−9, (b) group 10, and (c) group 11 metals (450 K, 1 bar $H_2$). Dashed lines are drawn to guide the eye. Free energy barriers ($\Delta G^{\ddagger}$) and tabulated data are shown in the Supporting Information (Figure S2 and Table S1; SI).

structure with wave-function convergence at $10^{-6}$ eV and an FFT grid 2× the planewave cutoff. After geometric convergence, a single-point calculation with an 8 × 8 × 1 sampling was performed to determine the electronic energy for all metals except for Co, which had convergence issues at a high *k*-point mesh. This three-step convergence significantly decreases the required cpu resources and is facilitated by CCI.[53] Co and Ni calculations were run spin-polarized because of their ferromagnetic properties. Transition-state structures for each elementary reaction were obtained by combining the nudged elastic band (NEB)[61,62] and dimer[63] methods. NEB calculations were run with 16 images and loosely converged to a force of 0.3 eV $Å^{-1}$ followed by a three-step dimer calculation similar to the optimizations described above. Frequency calculations were performed on gas-phase molecules and all optimized adsorbed species to determine zero-point vibrational energies (ZPVEs) and vibrational, translational, and rotational enthalpy and free energy. These terms were then used, together with electronic energies ($E_0$, provided by VASP), to estimate enthalpies ($H$) and free energies ($G$) for reactants, products, and transition states at 300−700 K. These vibrational frequency calculations also confirm, for transition states, the identity of a single imaginary frequency and identify the associated reaction mode. Converged structures on a metal surface can be used, with CCI,[53] to initiate calculations on any other metal surface, and this was done to accelerate this study of 10 close-packed metal surfaces.

To simplify analysis within this work, we assume that rates of C−X hydrogenolysis are limited by C−X bond cleavage rather than any dehydrogenation or hydrogenation events that may occur before or after that event. This assumption is supported by extensive data for C−C,[9−11,14] C−N,[31−34] C−O,[22] and C−Cl[46] hydrogenolysis. However, the C−S bond is much weaker than the other C−X bonds and may show comparable or lower barriers than C−H activations for certain pathways as have been shown previously using DFT on a Pt(111) surface.[44] Therefore, our rate analysis here (that assumes all C−H activations are quasi-equilibrated) reflects the maximum rate for C−S activation to allow a direct comparison of the bond's strength with the other C−X bonds. Furthermore, we assume that surfaces are essentially bare during reactions although one would expect H* to be an abundant surface intermediate at high $H_2$ pressures, and residues from the organic molecule such as C $H_x^*$, $NH_x^*$, $OH_x^*$, $SH_x^*$, Cl*, and CO* are likely (especially CO*) at low $H_2$ pressures. These assumptions allow this fundamental study to proceed, but we recognize, as we have done in past works,[28,29] that such assumptions make direct comparisons with experimental kinetic results more challenging. The effective enthalpy barrier ($\Delta H^{\ddagger}$) is thus defined as the enthalpy to form the partially dehydrogenated transition state for C−X cleavage (denoted here as $[CH_{(3-y)}-XH_{(n-z)}]^{\ddagger}$) and a stoichiometric amount of $H_2$(g) from gas-phase species ($CH_3XH_n$) and a bare surface

$$\Delta H^{\ddagger} = H[CH_{(3-y)}XH^{*}_{n-z}]^{\ddagger} + \lambda\, H[H_2(g)] - H[CH_3XH_n(g)] - H[*] \quad (1)$$

where $y$ and $z$ indicate the number of H removed for the $CH_3$ and $XH_n$ ends of the molecule and therefore $\lambda$ is the number of $H_2$(g) molecules evolved as a result of the dehydrogenation steps prior to transition-state formation

$$\lambda = 1/2\,(y + z) \quad (2)$$

Analogous equations for $\Delta S^{\ddagger}$ exist, where $\Delta S^{\ddagger}$ is dominated by the formation of gas-phase $H_2$ resulting from dehydrogenation prior to C−X cleavage. Effective free energy barriers, $\Delta G^{\ddagger}$, are obtained from their relation to $\Delta H^{\ddagger}$ and $\Delta S^{\ddagger}$

$$\Delta G^{\ddagger} = \Delta H^{\ddagger} - T\Delta S^{\ddagger} \quad (3)$$

The C−X bond cleavage turnover rate on bare surfaces can then be predicted by

$$\frac{r_y}{[L]} = \frac{k_B T}{h}\exp\left(\frac{-\Delta G^{\ddagger}}{RT}\right)\frac{(CH_3XH_n)}{(H_2)^{\lambda}} \quad (4)$$

assuming that C−H activation steps to form the partially dehydrogenated species are quasi-equilibrated and C−X activation is the rate-determining step, analogous to alkane hydrogenolysis. Further details of the computational methods can be found in the Supporting Information (Section S1, SI).



https://dx.doi.org/10.1021/acscatal.0c00481
ACS Catal. 2020, 10, 5086−5100

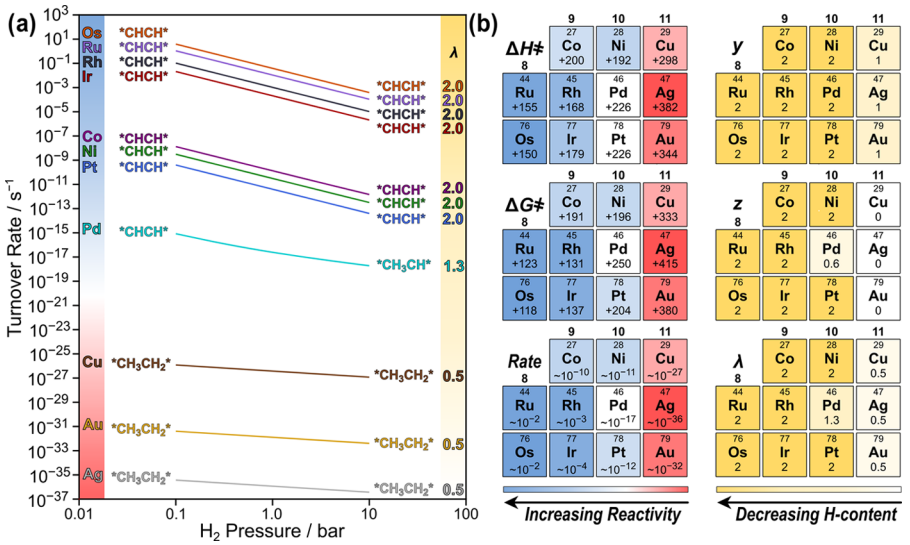


**Figure 2.** (a) DFT-predicted turnover rates for C−C bond cleavage as a function of $H_2$ pressure (eq 4; 450 K, 0.2 bar $CH_3CH_2$). Labels indicate the most favorable intermediates at low and high pressures. (b) Periodic trends in $\Delta H^{\ddagger}$, $\Delta G^{\ddagger}$, turnover rate, $y$ (H removed from C1), $z$ (H removed from C2), and $\lambda$ (eq 2) values.

## 3. RESULTS AND DISCUSSION

**3.1. C−C Bond Cleavage in $CH_3CH_3$.** In this section, we reanalyze our past work examining C−C bond hydrogenolysis in ethane; however, here we exclude the energy required to remove H* atoms from the group 8−10 surfaces (although H* is a known MASI at high $H_2$/alkane ratios)[9−11,14,64−66] to make direct comparisons with other C−X activations examined in this study over bare metal surfaces. In our previous studies,[14,28,29] we have shown that this approach does not alter the conclusions about the reactive intermediate that cleaves the C−C bond in ethane and, through a fortuitous cancellation of errors, does not significantly worsen the agreement of predicted and measured rates. The effective enthalpy barriers ($\Delta H^{\ddagger}$; eq 1) to cleave the C−C bond in ethane-derived intermediates over bare group 8−11 metals are shown in Figure 1. Ru can cleave the C−C bond in $*CH_3CH_2*$ with an effective enthalpy barrier of 195 kJ mol$^{-1}$ (Figure 1a), but this barrier decreases to 157 kJ mol$^{-1}$ for $*CH_3CH*$ activation before it increases dramatically to 224 kJ mol$^{-1}$ for $*CH_3C*$ activation, suggesting that cleaving the C−C in CH*-containing intermediates is more favorable. $*CH_2CH*$ activation is also more favorable than $*CH_2CH_2*$ and $*CH_2C*$ by 8 and 85 kJ mol$^{-1}$, respectively. However, *CHCH* activation shows the lowest effective enthalpy barrier among all other intermediates (155 kJ mol$^{-1}$). Other group 8−9 metals (Os, Rh, and Ir) exhibit similar trends, and *CHCH* activation enthalpies are far below those of any other ethane-derived intermediates, except for Co, which shows similar trends to group 10 metals. For group 10 metals (Ni, Pd, and Pt), the preference starts to shift to less dehydrogenated intermediates (Figure 1b). For example, cleaving the C−C bond in $*CH_3CH*$ or $*CH_3CH_2*$ is >20 kJ mol$^{-1}$ more favorable than *CH−CH* over these metals. Group 11 metals (Cu, Ag, and Au) predominantly cleave the C−C bond in the most saturated intermediate $*CH_3CH_2*$ (Figure 1c). Transition-state structures are shown in Figures S7−S17 in the Supporting Information (SI).

These enthalpic barriers, however, do not account for the entropy gain associated with the evolution of $H_2$(g) following the dehydrogenation of $*CH_3CH_3*$ on the metal surface and H* desorption. Turnover rates depend on differences in free energy barriers $\Delta G^{\ddagger}$, and thus increasing the $\Delta S^{\ddagger}$ decreases $\Delta G^{\ddagger}$ (eq 3) and, consequently, increases the predicted turnover rate (eq 4). The magnitude of this effect of $\Delta S^{\ddagger}$ depends on the reaction temperature. Furthermore, turnover rates depend inversely on $H_2$ pressure (eq 4), and increasing the value of $\lambda$ decreases the turnover rate, favoring C−X cleavage in less dehydrogenated intermediates. Figure 2a shows the total DFT-predicted rate (sum of turnover rates of C−C activation in each ethane-derived intermediate) as a function of $H_2$ pressure (0.1−10 bar $H_2$, 450 K) calculated using $\Delta G^{\ddagger}$ values (Table S1; SI). *CH−CH* activation exhibits the highest turnover rate among all other intermediates over group 8−9 metals over the entire $H_2$ pressure range examined here, leading to rates that depend on $H_2$ pressure as $[H_2]^{-2}$ ($\lambda = y = z = 2$; eqs 2 and 4). This is in agreement with the measured rate dependence on $H_2$ pressure ($r \sim [H_2]^{-3}$) on 0.7 nm Ir, 0.9 nm Rh, and 1.0 nm Ru catalysts[9] as well as on large 7 nm Ir clusters ($r \sim [H_2]^{-3.3}$)[14] taking into account the fact that C−C hydrogenolysis requires the removal of 2 H* atoms from the H*-covered surface (leading to a measured $\lambda$ value of ∼3 instead of 2) at these conditions (0.2 bar ethane, 2−20 bar $H_2$, 593 K).[28] Measured turnover rates increase with increasing Ir particle size from small 0.7 nm Ir clusters to the large 7 nm clusters despite DFT predictions, which suggest that under-coordinated sites (corners and edges of metal particles) are more prone to poisoning by $CH_x^*$ species[28] than terrace sites. Although the enthalpic barriers to cleave the C−C bond in $*CH_3CH_2*$ are lower than those of *CHCH* by >20 kJ mol$^{-1}$ over Ni and Pt, the removal of additional H atoms increases the entropy, thus rendering the free energy the lowest for *CHCH* activation, 26 kJ mol$^{-1}$ lower than that for the next most reactive intermediates, leading to turnover rates that also depend on $H_2$ pressure as $[H_2]^{-2}$ but with lower reactivity than group 8−9 metals (Figure 2a). $^1$C−$^2$C and $^2$C−$^2$C bonds in longer *n*-alkanes also cleave via *RCCR* intermediates, which lost 4 H atoms prior to C−C cleavage as shown previously on 0.7 nm Ir catalysts.[10,12] However, measured C−C activation turnover rates increase on increasing the chain length because longer alkanes are more stabilized by the attractive vdW


https://dx.doi.org/10.1021/acscatal.0c00481
ACS Catal. 2020, 10, 5086−5100

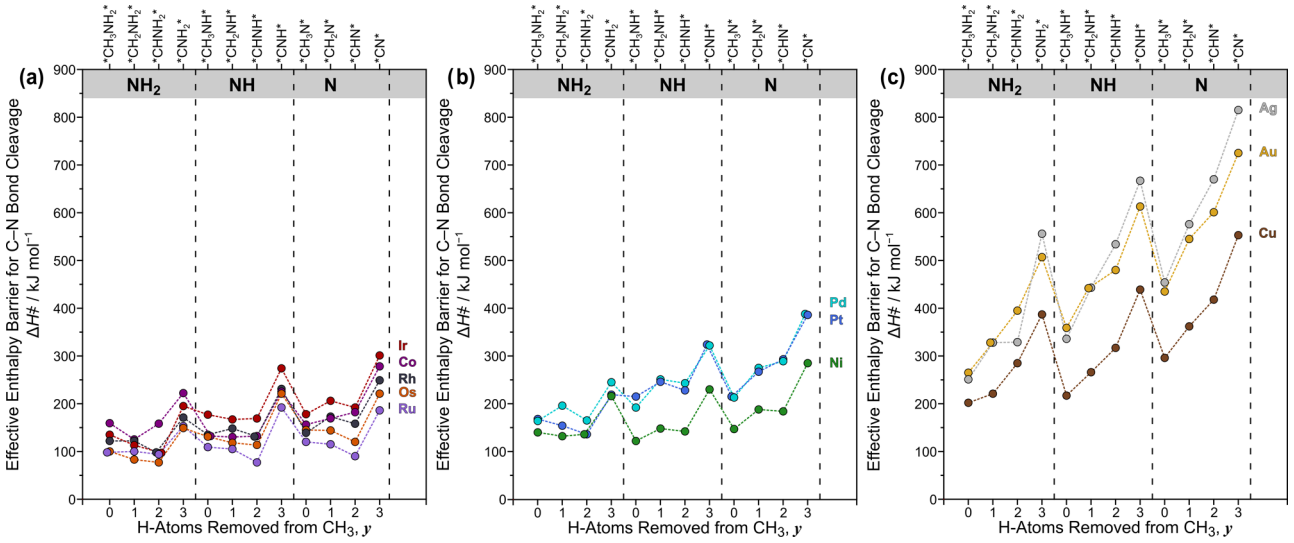


**Figure 3.** Effective enthalpy barriers ($\Delta H^{\ddagger}$; eq 1) for C−N bond cleavage in methylamine-derived intermediates on (a) groups 8−9, (b) group 10, and (c) group 11 metals (450 K, 1 bar $H_2$). Dashed lines are drawn to guide the eye. Free energy barriers ($\Delta G^{\ddagger}$) and tabulated data are shown in the Supporting Information (Figure S3 and Table S2; SI).

interactions between the transition state and the metal surface.[12] *CHCH* and *$CH_3$CH* activations on Pd have free energy barriers similar in magnitude (250 and 254 kJ $mol^{-1}$); thus, both intermediates can contribute equally to the predicted rate at 0.4 bar $H_2$, but at $H_2$ pressures >0.4 bar $H_2$, *$CH_3$CH* activation becomes more favorable, giving an average $\lambda$ value of 1.3 ($y$ = 2; $z$ = 0.6). Coinage metals are much less active and always cleave *$CH_3CH_2$* and show a $\lambda$ value of 0.5 ($y$ = 1; $z$ = 0). These findings suggest that catalytic activity and the extent of dehydrogenation required to cleave the C−C bond decrease as one moves from left to right in the periodic table (Figure 2b).

Generally, the rate of C−C hydrogenolysis decreases as one moves from left to right on the periodic table and from top to bottom, consistent with the more noble nature of metals in the bottom-right of the transition block and with the measured turnover rates that decrease as Ru > Rh > Ir > Pt.[9,10] There are, however, two notable exceptions: Pd and Ag. Pd is less reactive than Ni or Pt (the other group 10 metals) by roughly 6 orders of magnitude, consistent with a relative lack of literature data for alkane hydrogenolysis on Pd and in contrast to these established periodic trends. Similarly, Ag is less reactive than Au and Cu by 4−9 orders of magnitude, respectively, again defying typical periodic trends and indicating that period 5 metals, such as Pd and Ag, may be inherently bad at activating C−C bonds, likely because they bind $CH_x$* species more weakly than their period 6 counterparts and because of some peculiarity in their electronic structures as shown previously.[67,68]

**3.2. C−N Bond Cleavage in $CH_3NH_2$.** The effective enthalpy barriers ($\Delta H^{\ddagger}$; eq 1) to cleave the C−N bond in methylamine-derived intermediates over group 8−11 metals are shown in Figure 3. Adsorbed $CH_3NH_2$* on Ru(001), for example, can undergo C−N bond cleavage with an effective barrier of 98 kJ $mol^{-1}$ (Figure 3a,b). The effective barrier for methylamine dissociation decreases weakly as H atoms are removed from the $CH_3$ group (with the number of H removed denoted $y$) down to 94 kJ $mol^{-1}$ in *$CHNH_2$* ($y$ = 2; Figure 4c) before it increases significantly to 153 kJ $mol^{-1}$ in *$CNH_2$* ($y$ = 3; Figure 4d). Amino-methylidyne (*$CNH_2$*) is a stable

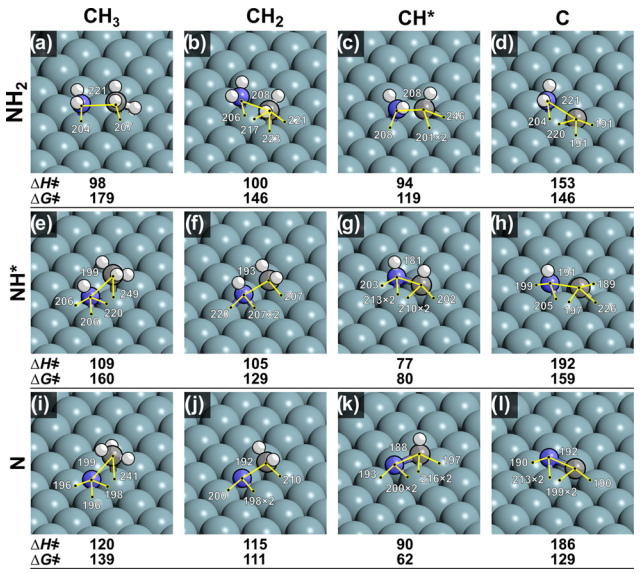


**Figure 4.** Transition-state structures for C−N bond cleavage in methylamine-derived intermediates on the Ru(001) surface. Shown beneath the images are $\Delta H^{\ddagger}$ and $\Delta G^{\ddagger}$ values in kJ $mol^{-1}$ (eq 1, 450 K, 1 bar $H_2$). Important bond distances are shown in pm. Similar images for the other examined metals are shown in the Supporting Information (Figures S18−S28; SI) along with their structures and reaction mode files.

surface intermediate that binds strongly on metal surfaces as previously reported on the Pt(111) surface,[69] consistent with its unfavorable C−N bond activation. C−N bond activation follows the same trend with the removal of one or two H atoms from the nitrogen atom ($z$ = 1 and 2, respectively), such that *$CHNH_{0-2}$* intermediates have the lowest C−N activation barriers (Figure 3a). *CHNH* has the lowest C−N activation barrier among all other intermediates by >13 kJ $mol^{-1}$, consistent with the preference of *CH−CH* activation in ethane hydrogenolysis.[29] Os(001) shows a similar preference toward cleaving the C−N bond in CH*-containing intermediates; however, C−N bond cleavage in *$CHNH_2$* is more favorable than in *CHNH* over Os (Figure 1a) by 34 kJ


https://dx.doi.org/10.1021/acscatal.0c00481
ACS Catal. 2020, 10, 5086−5100

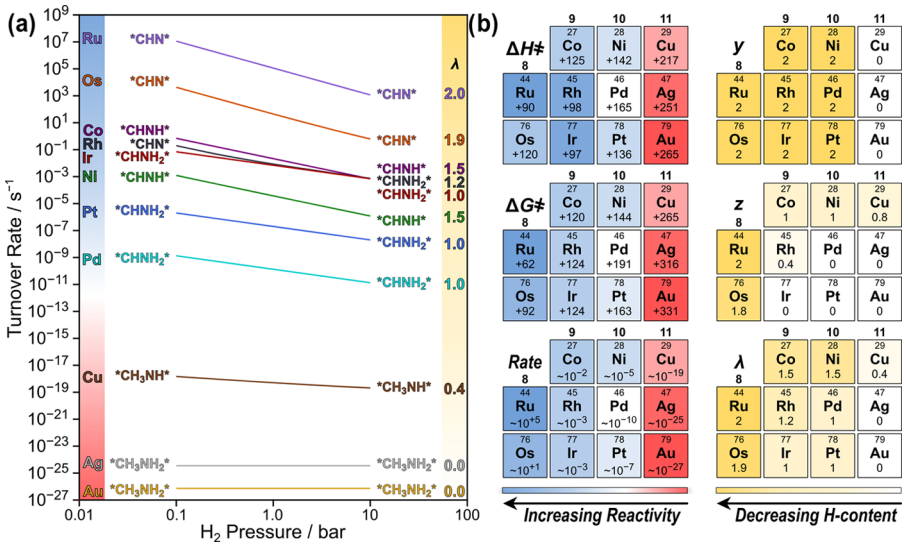


**Figure 5.** (a) DFT-predicted turnover rates for C−N bond cleavage as a function of $H_2$ pressure (eq 4; 450 K, 0.2 bar $CH_3NH_2$). Labels indicate the most favorable intermediates at low and high pressures. (b) Periodic trends in $\Delta H^{\ddagger}$, $\Delta G^{\ddagger}$, turnover rate, $y$ (H removed from C), $z$ (H removed from N), and $\lambda$ (eq 2) values.

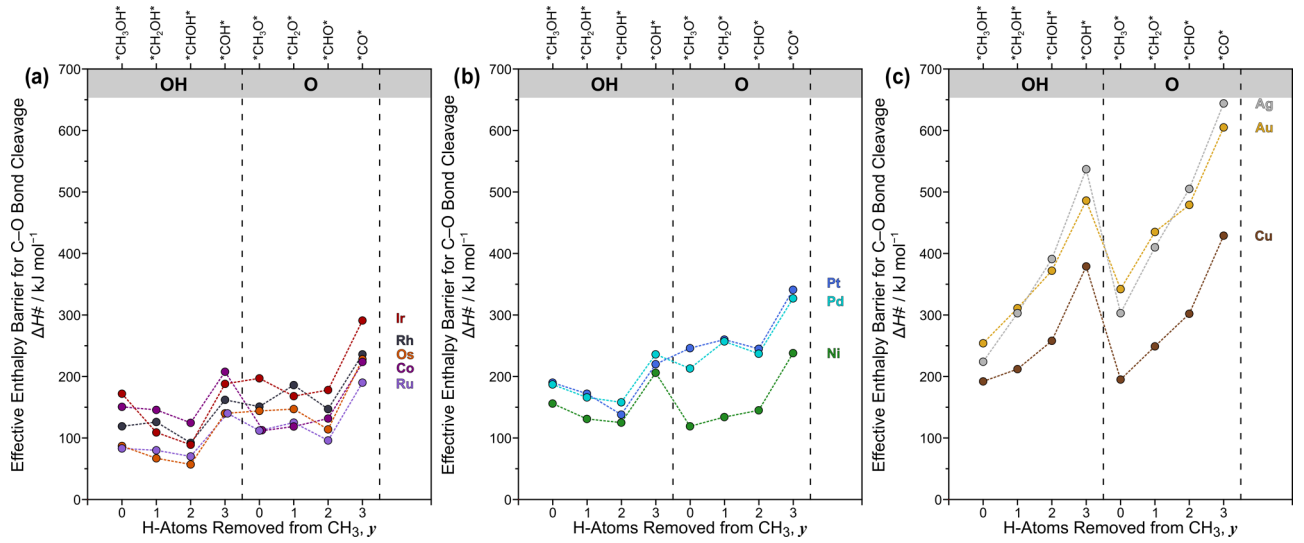


**Figure 6.** Enthalpy barriers ($\Delta H^{\ddagger}$; eq 1) for C−O bond cleavage in methanol-derived intermediates on (a) groups 8−9, (b) group 10, and (c) group 11 metals (450 K, 1 bar $H_2$). Dashed lines are drawn to guide the eye. Free energy barriers ($\Delta G^{\ddagger}$) and tabulated data are shown in the Supporting Information (Figure S4 and Table S3; SI).

$mol^{-1}$, in contrast to Ru. Group 9−10 metals (Co, Rh, Ir, Pd, Ni, Pd, and Pt) also prefer to cleave *$CHNH_2$* with the exception of Co and Ni, which show more preference toward *$CH_2NH_2$* and *$CH_3NH$*, respectively, and Pd can cleave *$CH_3NH_2$* with a similar barrier as *$CHNH_2$* (Figure 3a,b). Coinage metals (Cu, Ag, and Au), on the other hand, predominantly cleave *$CH_3NH_2$* with enthalpic barriers that range from 202 kJ $mol^{-1}$ on Cu to 265 kJ $mol^{-1}$ on Au (Figure 3c), approaching the measured gas-phase bond dissociation energy of $CH_3-NH_2$ (~350 kJ $mol^{-1}$),[5,6] and consistent with our previous findings for C−C hydrogenolysis in ethane.[29]

The total DFT-predicted rate as a function of $H_2$ pressure (Figure 5a) indicates that all group 8−10 metals favor cleaving the C−N bond in CH-containing intermediates, while coinage metals favor $CH_3$-containing intermediates over the examined $H_2$ pressure range. This common preference to form CH* upon cleaving the C−C bond in ethane and the C−N bond in methylamine indicates that the nitrogen atom in methylamine does not influence the preferred H-content on the carbon atom ($y$ = 2; Figure 5b). The H-content on the nitrogen atom, however, varies from $z$ = 0 ($NH_2$*) to $z$ = 2 (N*). Although *CH−NH* and *CH−$NH_2$* are enthalpically more favorable on Ru and Os (Figure 3a), respectively, *CH−N* becomes more favorable after considering the entropy gain (Table S2; SI) associated with the removal of additional H atoms (Figure 5a). Both *CH−N* and *CH−$NH_2$* have free energy barriers similar in magnitude on Rh (131 and 124 kJ $mol^{-1}$, respectively), and thus *CH−N* is more favorable at low $H_2$ pressures, while *CH−$NH_2$* is more favorable at high $H_2$ pressures (Figure 5a), giving an average $z$ value of ~0.4 (calculated using eq 2 given that $y$ = 2 and $\lambda$ = 1.2 from the fit in Figure 5a). The $z$ value is sensitive to both row and column in the periodic table, and generally, it decreases from left to right and from top to bottom (Figure 5b). For example, $z$


https://dx.doi.org/10.1021/acscatal.0c00481
ACS Catal. 2020, 10, 5086−5100

decreases from 2 on Ru (group 8) to 0.4 on Rh (group 9) to 0 on Pd and Ag (groups 10−11), and it also decreases from 0.8 on Cu (period 4) to 0 on Ag and Au (periods 5−6). This flexibility of the required H-content of nitrogen to cleave the C−N among these metals compared to carbon could be attributed to the nitrogen's lone pair of electrons, which allows the N atom to form different bonding geometries and bind without dehydrogenation depending on the electronic nature of the underlying metal. These findings indicate that the carbon atom always forms CH* upon C−N cleavage regardless of the identity of the metal surface within groups 8−10, while the nitrogen atom is more flexible.

The catalytic activity also decreases as one moves from left to right in the periodic table (Figure 5b), in agreement with the experimentally measured methylamine hydrogenolysis rates that decrease from group 7 to 10 metals[31−34] and consistent with our previous findings for alkane hydrogenolysis.[9,10,29] Notably, Ru has a particularly high rate of C−N cleavage (perhaps why it is a very active $NH_3$ synthesis catalyst because it can cleave the strong N≡N bond),[70−72] while Pd has a particularly low rate of C−N hydrogenolysis (similar to C−C bonds).

**3.3. C−O Bond Cleavage in $CH_3OH$.** The preferred H-content on the carbon atom for C−O activation in $CH_3OH$ follows the same trends as C−C and C−N activations (Figure 6): it prefers to lose two H atoms prior to C−O dissociation on group 8−10 metals and to lose no H atoms prior to C−O dissociation on group 11 metals. For example, the direct C−O activation in *$CH_3OH$* over Ru has an effective enthalpic barrier ($\Delta H^{\ddagger}$) of 83 kJ mol$^{-1}$ (Figure 7a), which decreases

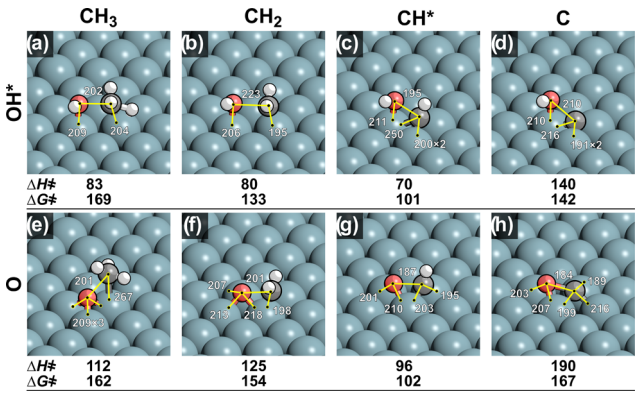


**Figure 7.** Transition-state structures for C−O bond cleavage in methanol-derived intermediates on the Ru(001) surface. Shown beneath the images are $\Delta H^{\ddagger}$ and $\Delta G^{\ddagger}$ values in kJ mol$^{-1}$ (eq 1, 450 K, 1 bar $H_2$). Important bond distances are shown in pm. Similar images for the other examined metals are shown in the Supporting Information (Figures S29−S39; SI) along with their structures and reaction mode files.

weakly down to 70 kJ mol$^{-1}$ in *CHOH* (Figure 7c) before it increases significantly to 140 kJ mol$^{-1}$ in *COH* (Figure 7d). C−O activation barriers in *$CH_{0-3}O$* intermediates exhibit a similar pattern, but they are 26−50 kJ mol$^{-1}$ higher than those for their analogous *$CH_{0-3}OH$* intermediates (Figure 6a), indicating that removing the H atom from oxygen is enthalpically unfavorable. These trends extend to all other group 8−9 metals (Os, Rh, and Ir) except for Co, where *$CH_{0-3}O$* intermediates are more enthalpically favorable. Although *CH−OH* activation remains favorable over group 10 metals (Ni, Pd, and Pt), removing the H atom from oxygen makes *$CH_3$−O* activation more favorable among *$CH_{0-3}O$* species over these metals (Figure 6b) and it is slightly more favorable than *CH−OH* activation (by 6 kJ mol$^{-1}$) on Ni. Au and Ag predominantly cleave *$CH_3$−OH* (Figure 6c), whereas *$CH_3$−O* activation competes with *$CH_3$−OH* activation on Cu (195 compared to 192 kJ mol$^{-1}$, respectively) similar to Ni, suggesting that cleaving the C−O bond in *$CH_{0-3}O$* intermediates starts to become more favorable as one moves from bottom to top in the periodic table.

DFT-predicted rates as a function of $H_2$ pressure (Figure 8a) calculated from the free energy barriers (Table 3; SI) indicate that C−O rupture occurs predominantly via the *CHOH* intermediate over group 8−10 metals at high $H_2$ pressures, consistent with the preference of cleaving the C−O bond in *$CH_3COH$* intermediates in ethanol on a Pt(111) surface.[36] For longer alkanols, however, deoxygenation via decarbonylation (i.e., RC−CO activation) to form CO* is more dominant than C−O hydrogenolysis at low CO* coverages as shown previously for 1-butanol on Ru, Ir, and Pt catalysts.[30] At intermediate $H_2$ pressures, *CH−O* and *CH−OH* contribute equally to the predicted turnover rate on Ru and Ni because they have similar free energy barriers. As $H_2$ pressure decreases, the effect of $H_2$ inhibition caused by the removal of additional H atoms ($\lambda$; eq 4) starts to weaken and thus *CH−O* becomes more favorable. For Co, however, *CH−O* activation is favorable at all conditions. Kinetic measurements at high $H_2$ pressures have shown that that ring-opening of 2-methyltetrahydrofuran ($C_5H_{10}O$) via the secondary C−O bond hydrogenolysis occurs after the removal of 2 H atoms from the $^2$C atom (i.e., RC*−O*$RCH_3$) on Ni.[22,23] *$CH_3$−O* activation has the highest turnover rate on Cu across the $H_2$ pressure range examined here, and, as expected, Ag and Au cleave *$CH_3$−OH* directly. Figure 8b shows that the catalytic activity also decreases from left to right in the periodic table and that removing 2 H atoms ($y = 2$) from carbon is required to cleave the C−O bond over group 8−10 metals, while group 11 metals only cleave C−O in $CH_3$-containing intermediates ($y = 0$). The H-content on oxygen is also influenced by the location of each metal within each group, such that the preference to activate *$CH_{0-3}$−O* intermediates appears to increase from period 6 to period 4. These periodic trends for C−O activation are analogous to C−N activation discussed in Section 3.2, where the carbon atom behaves similarly as in C−C activation, while the H-content on N and O can vary with both the group and period number of the metal catalyst.

Like C−C and C−N bond activations, C−O hydrogenolysis rates (on bare metals) generally decrease as one moves from left to right and from top to bottom of the periodic table, with a few exceptions. Ru is slightly less reactive than Os, and group 9 metals have essentially the same reactivity, despite Ru and Rh being higher on the periodic table than Os and Ir; moreover, Pd (as was observed for C−C and C−N bonds) is less reactive by 2−4 orders of magnitude than other group 10 metals.

**3.4. C−S Bond Cleavage in $CH_3SH$.** Sulfur is within the same group as oxygen, and thus one might expect C−S and C−O activations to have similar trends. However, effective enthalpy barriers ($\Delta H^{\ddagger}$; Figure 9) show that all examined metals cleave the C−S bond in *$CH_{0-3}S$* intermediates instead of *$CH_{0-3}SH$* intermediates, in contrast to C−O bond cleavage, where activating *$CH_{0-3}OH$* intermediates is generally more favorable. For example, the average C−S


https://dx.doi.org/10.1021/acscatal.0c00481
ACS Catal. 2020, 10, 5086−5100

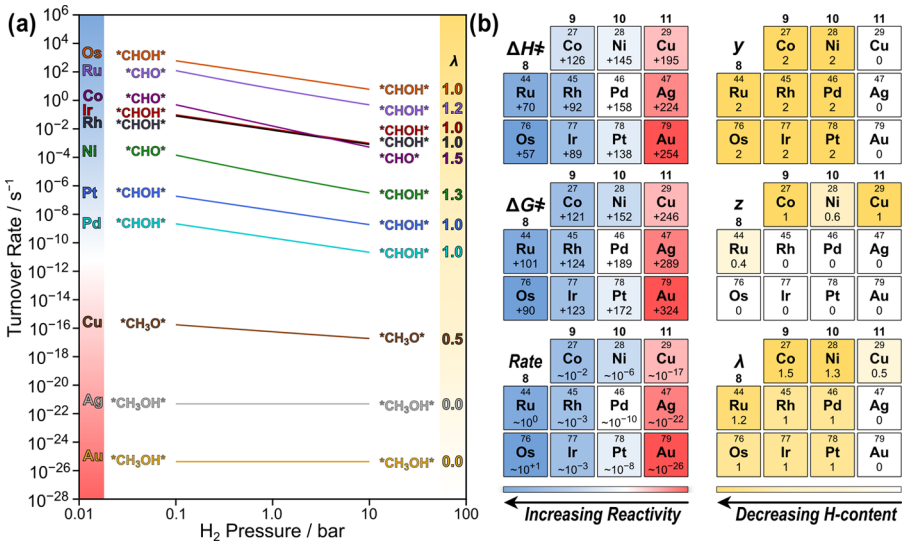


**Figure 8.** (a) DFT-predicted turnover rates for C−O bond cleavage as a function of $H_2$ pressure (eq 4; 450 K, 0.2 bar $CH_3OH$). Labels indicate the most favorable intermediates at low and high pressures. (b) Periodic trends in $\Delta H^{\ddagger}$, $\Delta G^{\ddagger}$, turnover rate, $y$ (H removed from C), $z$ (H removed from O), and $\lambda$ (eq 2) values.

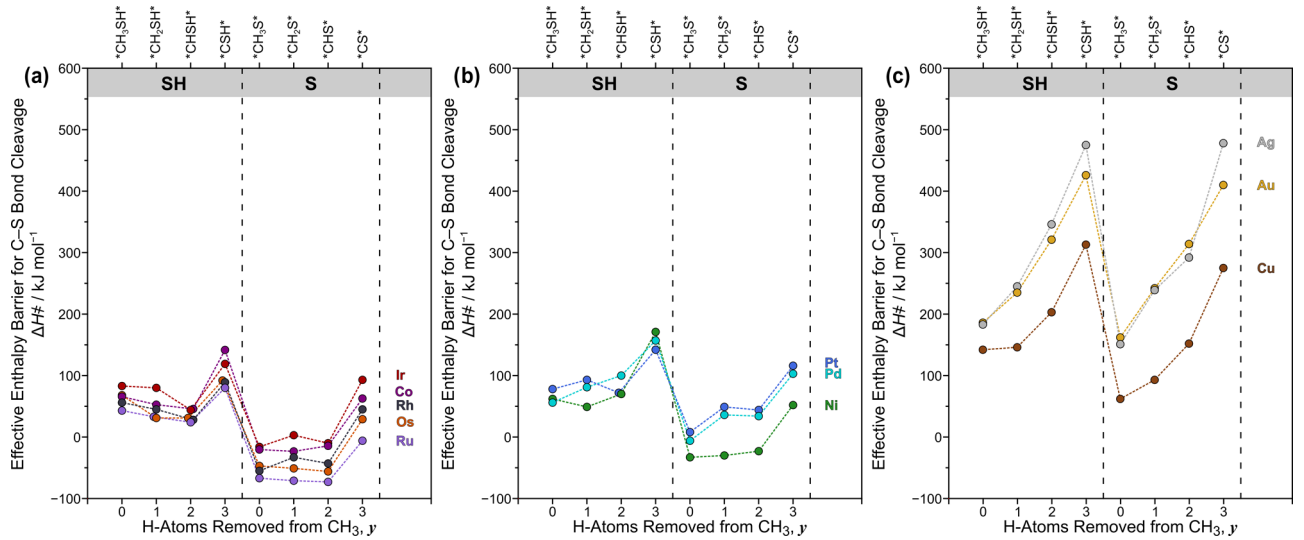


**Figure 9.** Enthalpy barriers ($\Delta H^{\ddagger}$; eq 1) for C−S bond cleavage in methanethiol-derived intermediates on (a) groups 8−9, (b) group 10, and (c) group 11 metals (450 K, 1 bar $H_2$). Dashed lines are drawn to guide the eye. Free energy barriers ($\Delta G^{\ddagger}$) and tabulated data are shown in the Supporting Information (Figure S5 and Table S4; SI).

activation enthalpy barrier in *$CH_{0-3}SH$* over Ru is 45 kJ mol$^{-1}$ compared to an average of −59 kJ mol$^{-1}$ for *$CH_{0-3}S$* activation (Figure 10). *CHS* activation remains enthalpically favorable over Ru and Os (group 8); however, this preference starts to shift toward *$CH_3S$* activation over Co, Rh, and Ir (group 9). The *$CH_3S$* activation barrier is lower than *CHS* activation by 12 kJ mol$^{-1}$ over Rh and by 6 kJ mol$^{-1}$ over Co and Ir. This preference for *$CH_3$−S* continues to increase in group 10 metals, where it is >36 kJ mol$^{-1}$ more favorable than *CH−S* on Pd and Pt (Figure 9b). However, *$CH_3$−S* and *CH−S* remain within 10 kJ mol$^{-1}$ over Ni, similar to group 9 metals, suggesting that *$CH_3$−S* becomes more favorable with increasing group and period number of the metal catalyst (moving from left to right and top to bottom). Notably, even group 11 metals (Cu, Ag, Au) cleave *$CH_3S$* instead of the most H-saturated intermediate *$CH_3SH$*, indicating that SH*-containing intermediates are highly unstable compared to *ROH*. Temperature-programmed reaction (TPR) and X-ray photoelectron spectroscopy (XPS) studies have shown that the S−H bond in alkanethiols breaks readily upon adsorption to form alkyl thiolate on Pt, Ni, and Mo surfaces.[73−77]

The DFT-predicted turnover rate for *CH−S* activation over group 8−9 metals is at least several orders of magnitudes (>$10^3$) higher than that for the next most reactive intermediate (*$CH_3S$*) over the entire pressure range examined in this study; thus, these other C−S cleavage routes are unlikely to contribute to the measured rate at these conditions (Figure 11a). The C−S activation rate is dominated by the *CHS* intermediate on Co, Rh, Ir, and Ni despite the enthalpic preference to cleave *$CH_3S$* on these metals (Figure 9) as a result of entropy differences, which are reflected in the differences in free energy barriers (Table 4; SI). However, these entropic gains cannot offset the large differences in


https://dx.doi.org/10.1021/acscatal.0c00481
ACS Catal. 2020, 10, 5086−5100

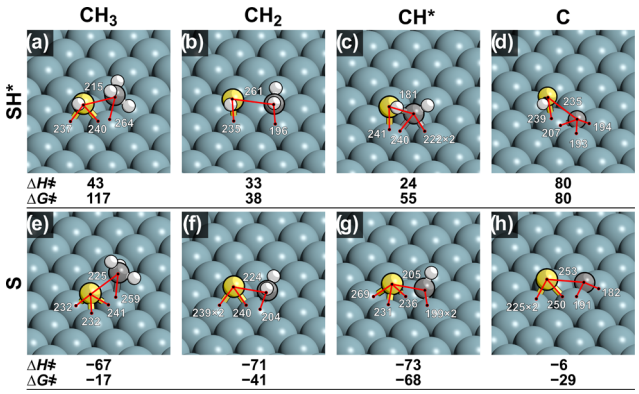


**Figure 10.** Transition-state structures for C−S bond cleavage in methanethiol-derived intermediates on the Ru(001) surface. Shown beneath the images are $\Delta H^{\ddagger}$ and $\Delta G^{\ddagger}$ values in kJ mol$^{-1}$ (eq 1, 450 K, 1 bar $H_2$). Important bond distances are shown in pm. Similar images for the other examined metals are shown in the Supporting Information (Figures S40−S50; SI) along with their structures and reaction mode files.

activation enthalpies between *CHS* and *$CH_3$S* activations on Pd and Pt (>36 kJ mol$^{-1}$; Figure 9b), rendering $\Delta G^{\ddagger}$ values for these two routes similar. As a result, *$CH_3$S* activation becomes more favorable on Pd and Pt at high $H_2$ pressures because deeply dehydrogenated intermediates are inhibited by $H_2$ to a greater extent (eq 4). These findings are consistent with previous DFT studies that show that S−H activation is facile over Pt(111) and that C−S cleavage in methanethiol occurs via the *CHS* intermediate under ultrahigh vacuum conditions and via *$CH_3$S* under hydrogenation conditions.[44] Group 11 metals (Cu, Ag, and Au) predominantly cleave *$CH_3$−S* at all $H_2$ pressures but with significantly lower reactivity, leading to periodic trends for reactivity (rate; Figure 11b) and extent of dehydrogenation ($y$ and $\lambda$; Figure 11b) that decrease from left to right and from top to bottom in the periodic table.

**3.5. C−Cl Bond Cleavage in $CH_3Cl$.** Chlorine is within group 17 and forms one bond only with carbon in chloromethane ($CH_3Cl$); thus, the removal of H atoms from C−Cl can only occur from the carbon atom. Adsorbed *$CH_3Cl$* can undergo a direct *$CH_3$−Cl* bond activation on Ru with an effective enthalpic barrier of 72 kJ mol$^{-1}$ (Figures 12a and 13a), but it decreases dramatically to 35 kJ mol$^{-1}$ for *$CH_2$−Cl* (Figure 13c) and 39 kJ mol$^{-1}$ for *CH−Cl* (Figure 13c) before it increases back to 54 kJ mol$^{-1}$ for *C−Cl* (Figure 13d). Os, Rh, and Ir exhibit a similar trend where *$CH_2$−Cl* activation has the lowest activation barrier, slightly lower than the *CH−Cl* activation barrier (by 13 kJ mol$^{-1}$ on average). Group 10 metals (Ni, Pd, and Pt) in addition to Co, however, do not show a clear trend (Figure 12b). For example, *$CH_3$−Cl* activation is >11 kJ mol$^{-1}$ more favorable than *$CH_2$−Cl* on Ni and Co, *CH−Cl* is the most favorable on Pd, and *$CH_2$−Cl* is the most favorable on Pt. Coinage metals predominantly activate *$CH_3$−Cl* except for Cu, where the *$CH_2$−Cl* activation barrier is only 8 kJ mol$^{-1}$ higher than *$CH_3$−Cl* (Figure 12c).

The calculated free energy barriers at 450 K (Table 3; SI) indicate that *C−Cl* activation is 11 kJ mol$^{-1}$ more favorable than *CH−Cl* over Ru and thus the *C−Cl* activation turnover rate is faster than *CH−Cl* activation by at least an order of magnitude over the examined $H_2$ pressure range (Figure 14a). Os shows a competition between *C−Cl* and *CH−Cl*, where *C−Cl* is favorable at low $H_2$ pressures, while *CH−Cl* is more favorable at high pressures because the difference in their $\Delta G^{\ddagger}$ values is <10 kJ mol$^{-1}$. *CHCl* is the dominant C−Cl activation intermediate on all group 8−9 metals (Co, Rh, Ir, Ni, Pd, and Pt), and thus total rates show a $H_2$ pressure dependence on $[H_2]^{-1}$ ($\lambda$ = 1). Coinage metals favor C−Cl activation in *$CH_3Cl$*, but, notably, Cu starts to behave more like group 10 metals and can cleave the C−Cl bond in *$CH_2Cl$* instead of *$CH_3Cl$* at low $H_2$ pressures. TPR and XPS studies of hydrodechlorination of 1,2-dichloroethane on Pd(100) and Cu(100) surfaces show that Pd is much more active than Cu but less selective toward ethylene.[78] Taken together, these trends indicate that the required H-content on the carbon atom to cleave the C−Cl in

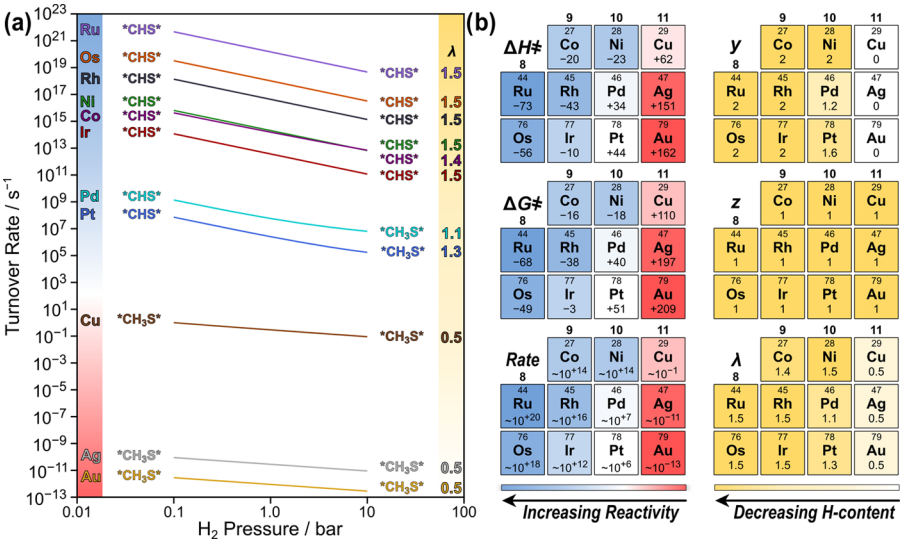


**Figure 11.** (a) DFT-predicted turnover rates for C−S bond cleavage as a function of $H_2$ pressure (eq 4; 450 K, 0.2 bar $CH_3SH$). Labels indicate the most favorable intermediates at low and high pressures. (b) Periodic trends in $\Delta H^{\ddagger}$, $\Delta G^{\ddagger}$, turnover rate, $y$ (H removed from S), $z$ (H removed from N), and $\lambda$ (eq 2) values.



https://dx.doi.org/10.1021/acscatal.0c00481
ACS Catal. 2020, 10, 5086−5100

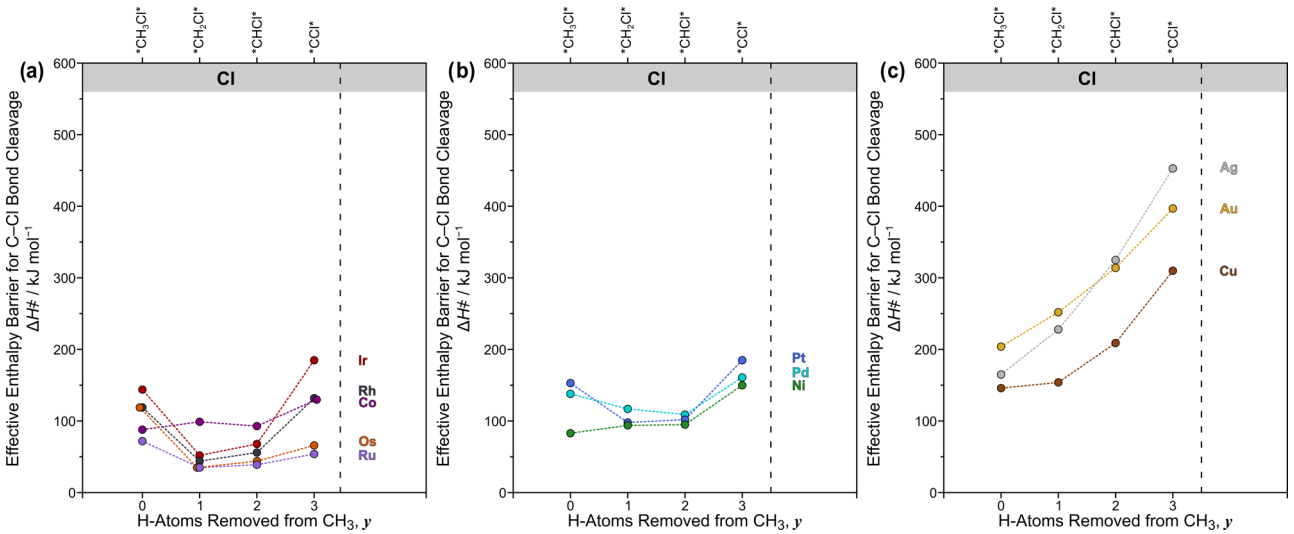


**Figure 12.** Enthalpy barriers ($\Delta H^{\ddagger}$; eq 1) for C−Cl bond cleavage in chloromethane-derived intermediates on (a) groups 8−9, (b) group 10, and (c) group 11 metals (450 K, 1 bar $H_2$). Dashed lines are drawn to guide the eye. Free energy barriers ($\Delta G^{\ddagger}$) and tabulated data are shown in the Supporting Information (Figure S6 and Table S5; SI).

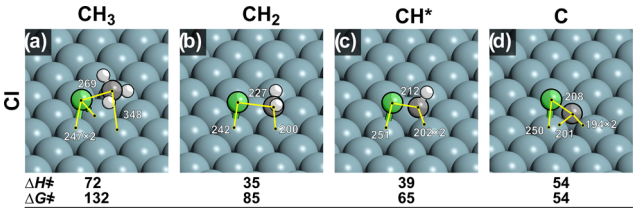


**Figure 13.** Transition-state structures for C−Cl bond cleavage in chloromethane-derived intermediates on the Ru(001) surface. Shown beneath the images are $\Delta H^{\ddagger}$ and $\Delta G^{\ddagger}$ values in kJ $mol^{-1}$ (eq 1, 450 K, 1 bar $H_2$). Important bond distances are shown in pm. Similar images for the other examined metals are shown in the Supporting Information (Figures S51−S61; SI) along with their structures and reaction mode files.

chloromethane and the catalytic activity decrease on increasing the group number of the transition metal (Figure 14b).

### 3.6. Contrasting C−X Cleavage.

Figure 15 summarizes the key findings in this study of C−X bond cleavage (X = C, N, O, S, and Cl) and the observed periodic trends. The carbon atoms in C−X hydrogenolysis prefer to cleave after the removal of 2 H atoms ($y$ = 2), but this value starts to decrease on increasing the group number of the transition metal down to $y$ = 0 for unreactive coinage metals and increase on increasing the group number of the heteroatom. The slight decrease in the number of H atoms that must be removed from the C atom on group 10 metals (Ni, Pd, and Pt) is attributed to the competition of multiple reactive intermediates that differ in their H-content (e.g., *CHS* with *$CH_3$S* for C−S activation, and *CHCH* with *$CH_3$CH* for C−C activation). The Cl atom in $CH_3Cl$ can only form a single bond with C and does not have H atoms to lose; thus, reactive group 8 metals such as Ru and Os can cleave the C−Cl after the removal of an additional H atom ($y$ = 3) from the C atom

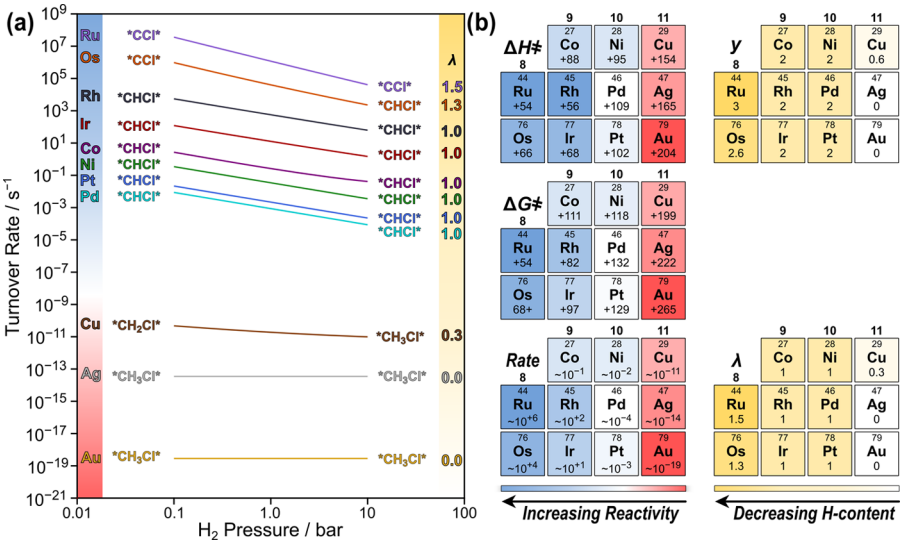


**Figure 14.** (a) DFT-predicted turnover rates for C−Cl bond cleavage as a function of $H_2$ pressure (eq 4; 450 K, 0.2 bar $CH_3Cl$). Labels indicate the most favorable intermediates at low and high pressures. (b) Periodic trends in $\Delta H^{\ddagger}$, $\Delta G^{\ddagger}$, turnover rate, $y$ (H removed from C), $z$ (H removed from Cl), and $\lambda$ (eq 2) values.



https://dx.doi.org/10.1021/acscatal.0c00481
ACS Catal. 2020, 10, 5086−5100

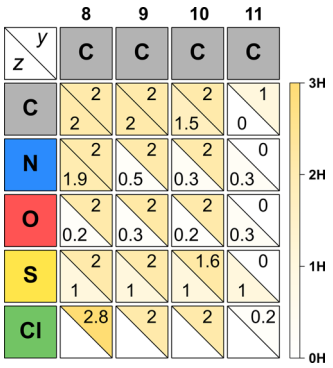


**Figure 15.** Average number of H atoms removed from C (top; $y$) and X (left; $z$) for each metal group (450 K, 0.2 bar $CH_3X_n$).

(i.e., in *CCl*), and even Cu starts to favor less saturated intermediates. The preferred H-content of N in C−N activation ($z$) varies significantly and is affected by both row and column of these transition metals. However, in general, it decreases on increasing both group and period number. Most transition metals cleave the C−O bond in OH*-containing intermediates ($z$ = 0) at high $H_2$ pressure, but O*-containing intermediates ($z$ = 1) start to compete at low pressures, leading to average $z$ values of 0.2−0.3, while the S atom in C−S activation always leaves as S* ($z$ = 1) regardless of the identity of the metal catalyst.

Generally, the reactivity of C−X bonds decreases from left to right and from top to bottom on the periodic table. The relative rates of C−X bonds as the X atom changes depend primarily on the bond dissociation energies, which decrease for $CH_3-XH_n$ cleavage on the order of OH > $CH_3$ > $NH_2$ > Cl > SH, as shown in Figure 16; however, some notable deviations from that general trend are observed. Most prominently, while the bond dissociation energy of $CH_3OH$ is 10 kJ $mol^{-1}$ higher than that of $CH_3CH_3$ (consistent with prior reports),[5] the rates

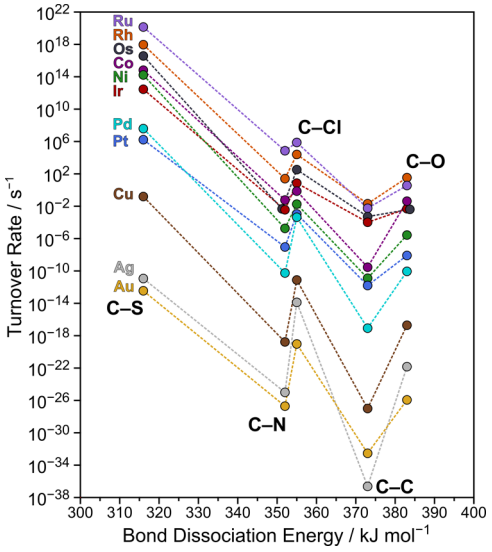


**Figure 16.** DFT-predicted turnover rate dependence on the bond dissociation energy of $CH_3-XH_n$ in the gas phase ($CH_3SH$: 316 kJ $mol^{-1}$; $CH_3NH_2$: 352 kJ $mol^{-1}$; $CH_3Cl$: 355 kJ $mol^{-1}$; $CH_3CH_3$: 373 kJ $mol^{-1}$; $CH_3OH$: 383 kJ $mol^{-1}$) for each examined metal (eq 4; 450 K, 1 bar $H_2$, 0.2 bar $CH_3XH_n$). Dashed lines are drawn to guide the eye.

of C−O activation are $10-10^{10}$ times higher than the rates of C−C hydrogenolysis at the same conditions and catalyst, indicating that catalyst surfaces stabilize O moieties to a greater extent than $CH_x^*$ fragments (relative to gas-phase radicals). C−O hydrogenolysis is particularly favored (relative to C−C hydrogenolysis) on coinage metals with rates $10^6-10^{10}$ higher than C−C activation, while group 8−10 metals are less selective toward C−O relative to C−C with C−O activation rates that are only $10-10^7$ faster than those for C−C.

**3.7. Linear Free Energy Relationships.** Sabatier-based approaches such as Brønsted−Evans−Polanyi (BEP)-type relations,[79−82] scaling relations,[83] or the d-band model[84,85] have been used as tools to predict the reactivity on different metal catalysts based on reactants, products, or atomic binding energies (descriptors), which are computationally less expensive calculations than transition-state calculations.[86−93] These correlations can be developed from examining a set of metal catalysts and then can be used to screen many other potential catalysts. Although this study does not aim to screen catalytic materials because our study neglects the influence of coverage, which will dominate the chemistry involving S, Cl, and often O, we assess here how accurately Sabbatier-based relationships hold for such reactions and whether they can be used to predict the trends in reactivity and the relative preferences among C−X activations.

Figure 17 shows the correlations between the DFT-predicted turnover rates calculated from the effective free energy barriers $\Delta G^{\ddagger}$ for each metal (eq 4; 450 K, 1 bar $H_2$, 0.2 bar $CH_3XH_n$) and (a) the formation free energy of the products C* + X* and the stoichiometric amount of $H_2$(g) relative to $CH_3XH_n$(g), and (b) the binding free energy of X* relative to the X•(g) radical. In general, the formation energy of C* + X* better describes the trends in reactivity among transition metals than the simple binding energy of X* because the products C* + X* have more similar compositions and structure to the C−X activation transition state than X* only. Notably, the binding energy of S* describes C−S activation trends very well (Figure 17b) because of the universal preference to form S* upon C−S bond cleavage in $*CH_{0-3}S*$ intermediates on all metals, unlike C−N and C−O activations, where the preferred H-content on X* varies across the metals, or C−C activation, where almost all metals form CH* instead of C*. Although C−Cl activation on all metals also forms Cl* similar to the formation of S* in C−S activation, Cl* binds and interacts with the metal surface very weakly during C−Cl activation compared to S*, and thus the binding energy of Cl* is a poor descriptor in this case (Figure 17b). The relative binding energies of X* also do not predict the relative rates of C−X activation since C−S activation shows the highest rates compared to any other C−X activations, but S* has an intermediate binding energy between C* and Cl* (Figure 17b). These linear relations can be useful in screening thousands of potential catalysts, but their apparent accuracy is exaggerated by the inclusion of coinage metals and the 60 orders of magnitude range in turnover rates in these plots.

Although this study focuses on simple substrates, this is the first step toward a broader understanding of the mechanisms of heteroatom removal in more complex molecules. Future studies will contrast these primary C−X activations with those of secondary and tertiary carbon atoms as well as longer chain lengths to contrast C−C and C−X activation within the same molecule. Previous works have shown that C−CO bond


https://dx.doi.org/10.1021/acscatal.0c00481
ACS Catal. 2020, 10, 5086−5100

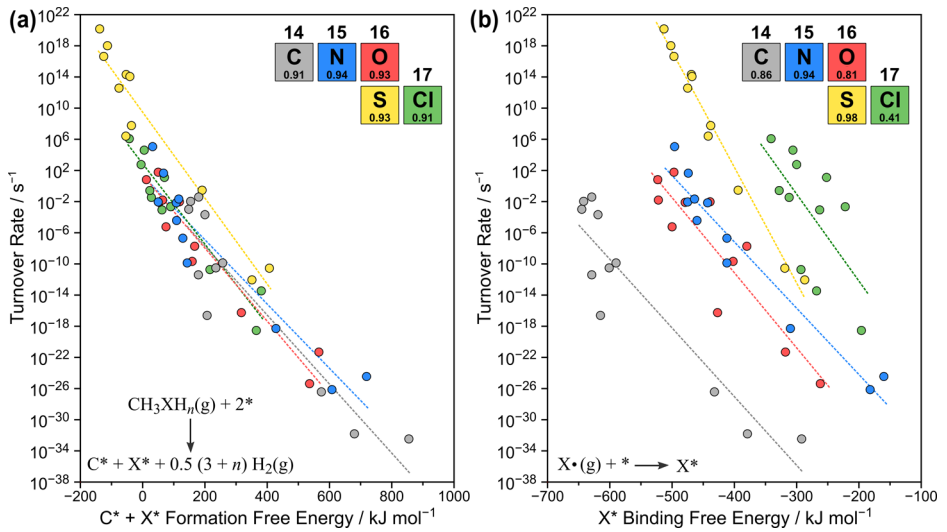


**Figure 17.** DFT-predicted turnover rate dependence (eq 4; 450 K, 1 bar $H_2$, 0.2 bar $CH_3XH_n$) on (a) the formation free energy of C* + X* and the stoichiometric amount of $H_2$(g) relative to $CH_3XH_n$(g) and a bare surface and (b) binding free energy of X* relative to the X•(g) radical. The $R^2$ values for each fit are shown in the legend.

activation in 1-butanol (i.e., decarbonylation), for example, is more favorable than C−O bond activation on Ru, Ir, and Pt, while Cu preferentially cleaves the C−O bond.[30] We have also shown previously that tertiary $^3$C−$^1$C hydrogenolysis in isobutane requires the removal of H atoms from other carbon atoms not involved in $^3$C−$^1$C bond cleavage.[13] 2-Propanol, 2-propanethiol, and 2-propanamine, for example, have similar structures to isobutane, but it is unknown whether these $^3$C−X bonds can be cleaved in a similar manner to $^3$C−$^1$C bond cleavage in isobutane or whether they exhibit different mechanisms, which will be examined in a future work. These are two examples of how we can construct a set of guiding principles, which will give insights into relative rates and mechanisms of various hydrogenolysis reactions of more complex substrates on different metal surfaces.

## 4. CONCLUSIONS

We have shown in our previous study that C−C hydrogenolysis in ethane occurs predominantly via the *CHCH* intermediate, which lost 2 H atoms from each carbon atom over group 8−10 metals (Ru, Os, Co, Rh, Ir, Ni, Pd, and Pt), while group 11 metals (Cu, Ag, and Au) activate the C−C bond in the most saturated intermediates with high free energy barriers closer to thermal activation of $CH_3CH_3$. Here, we extended our previous study to cover C−X bond cleavage (X = N, O, S, and Cl) in methylamine, methanol, methanethiol, and chloromethane over groups 8−11 to examine the periodic trends for the degree of unsaturation required to cleave the C−X bond. DFT-predicted free energy barriers and turnover rates at 450 K and $H_2$ pressure range of 0.1−10 bar indicate that the preferred number of H atoms that must be removed from carbon remains at $y$ = 2 (forming CH* upon cleavage) over group 8−10 metals and $y$ = 0 for group 11 metals, but it decreases slightly (∼1.6) for group 10 metals because different intermediates with more H-content start to contribute equally with *$CHXH_n$* intermediates to the total bond cleavage rate. This value of $y$ also increases slightly on increasing the group number of the heteroatom to $y$ = 2.8 for C−Cl activation over group 8 metals.

Although the C−N in methylamine is cleaved via *$CHNH_{2-z}$* intermediates over group 8−10 metals, the $z$ value decreases from $z$ = 2 on group 8 metals to $z$ = 0 on group 11 metals and decreases from $z$ = 1 on period 4 to $z$ = 0 on period 6, suggesting that N is more sensitive than C to the group and period number of the metal catalyst. The C−O bond in methanol generally prefers to cleave via *CHOH* intermediates ($y$ = 2; $z$ = 0), but *CHO* activation ($y$ = 2; $z$ = 1) is more favorable on Co and becomes more favorable at low $H_2$ pressures on Ru and Ni. C−S activation in methanethiol, however, predominantly occurs via *$CH_{1-3}S$* intermediates ($z$ = 1), indicating that SH*-containing intermediates are significantly unstable over all metals examined. The lack of H atoms in the Cl atom during C−Cl activation increases the preference to remove an additional H atom from the carbon atom compared to C−C, −N, −O, and −S activations, such that Ru favors *C−Cl* activation instead of *CH−Cl* and Cu favors *$CH_2$−Cl* instead of *$CH_3$−Cl*. This study on C−X activation in simple organic molecules, along with future work examining the effects of chain length and branching, may provide insights and guidance in predicting the mechanism and selectivities (relative rates) of C−X bond cleavage and provide a roadmap to a broader understanding of how more complex organic molecules with multiple functional groups will react on metal surfaces.

## ■ ASSOCIATED CONTENT

### Supporting Information

The Supporting Information is available free of charge at https://pubs.acs.org/doi/10.1021/acscatal.0c00481.

Transition-state structures and reaction mode files (ZIP)
Details of DFT calculations, $\Delta G^{\ddagger}$ figures, tabulated $\Delta H^{\ddagger}$, $\Delta G^{\ddagger}$, and $\Delta S^{\ddagger}$ values, and transition-state images (PDF)

## ■ AUTHOR INFORMATION

### Corresponding Author

**David D. Hibbitts** − *Department of Chemical Engineering, University of Florida, Gainesville, Florida 32611, United States;* orcid.org/0000-0001-8606-7000; Email: hibbitts@che.ufl.edu



https://dx.doi.org/10.1021/acscatal.0c00481
*ACS Catal.* 2020, 10, 5086−5100

## Author

**Abdulrahman S. Almithn** − *Department of Chemical Engineering, University of Florida, Gainesville, Florida 32611, United States; Department of Chemical Engineering, King Faisal University, Al-Ahsa 31982, Saudi Arabia*

Complete contact information is available at: https://pubs.acs.org/10.1021/acscatal.0c00481


## Notes

The authors declare no competing financial interest.

## ■ ACKNOWLEDGMENTS

D.D.H. acknowledges Profs. David Flaherty (University of Illinois, Urbana−Champaign) and Enrique Iglesia (University of California, Berkeley) for helpful discussions. A.S.A. acknowledges Saudi Arabian Cultural Mission (SACM) and King Faisal University, Saudi Arabia, for funding his graduate studies and research. Computational resources were provided by University of Florida Research Computing and the Extreme Science and Engineering Discovery Environment (XSEDE; CTS160041). Manuscript reviews and proofreading from Alexander Hoffman and Mykela DeLuca (University of Florida) are gratefully acknowledged.

## ■ REFERENCES


(1) Park, C.; Menini, C.; Valverde, J. L.; Keane, M. A. Carbon−chlorine and Carbon−bromine Bond Cleavage in the Catalytic Hydrodehalogenation of Halogenated Aromatics. *J. Catal.* **2002**, *211*, 451−463.

(2) Aramendía, M. A.; Boráu, V.; García, I. M.; Jiménez, C.; Lafont, F.; Marinas, A.; Marinas, J. M.; Urbano, F. J. Influence of the Reaction Conditions and Catalytic Properties on the Liquid-Phase Hydrodechlorination of Chlorobenzene over Palladium-Supported Catalysts: Activity and Deactivation. *J. Catal.* **1999**, *187*, 392−399.

(3) Hashimoto, Y.; Uemichi, Y.; Ayame, A. Low-temperature Hydrodechlorination Mechanism of Chlorobenzenes over Platinum-supported and Palladium-supported Alumina Catalysts. *Appl. Catal., A* **2005**, *287*, 89−97.

(4) Schrick, B.; Blough, J. L.; Jones, A. D.; Mallouk, T. E. Hydrodechlorination of Trichloroethylene to Hydrocarbons Using Bimetallic Nickel−iron Nanoparticles. *Chem. Mater.* **2002**, *14*, 5140−5147.

(5) Blanksby, S. J.; Ellison, G. B. Bond Dissociation Energies of Organic Molecules. *Acc. Chem. Res.* **2003**, *36*, 255−263.

(6) Kerr, J. A. Bond Dissociation Energies by Kinetic Methods. *Chem. Rev.* **1966**, *66*, 465−500.

(7) Luo, Y.-R. *Handbook of Bond Dissociation Energies in Organic Compounds*; CRC Press, 2002.

(8) Mó, O.; Yáñez, M.; Eckert-Maksić, M.; Maksić, Z. B.; Alkorta, I.; Elguero, J. Periodic Trends in Bond Dissociation Energies. A Theoretical Study. *J. Phys. Chem. A* **2005**, *109*, 4359−4365.

(9) Flaherty, D. W.; Iglesia, E. Transition-state Enthalpy and Entropy Effects on Reactivity and Selectivity in Hydrogenolysis of N-alkanes. *J. Am. Chem. Soc.* **2013**, *135*, 18586−18599.

(10) Flaherty, D. W.; Hibbitts, D. D.; Iglesia, E. Metal-catalyzed C-C Bond Cleavage in Alkanes: Effects of Methyl Substitution on Transition-state Structures and Stability. *J. Am. Chem. Soc.* **2014**, *136*, 9664−9676.

(11) Flaherty, D. W.; Uzun, A.; Iglesia, E. Catalytic Ring Opening of Cycloalkanes on Ir Clusters: Alkyl Substitution Effects on the Structure and Stability of C−C Bond Cleavage Transition States. *J. Phys. Chem. C* **2015**, *119*, 2597−2613.

(12) Hibbitts, D. D.; Flaherty, D. W.; Iglesia, E. Effects of Chain Length on the Mechanism and Rates of Metal-catalyzed Hydrogenolysis of N-alkanes. *J. Phys. Chem. C* **2016**, *120*, 8125−8138.

(13) Hibbitts, D. D.; Flaherty, D. W.; Iglesia, E. Role of Branching on the Rate and Mechanism of C−C Cleavage in Alkanes on Metal Surfaces. *ACS Catal.* **2016**, *6*, 469−482.

(14) Flaherty, D. W.; Hibbitts, D. D.; Gürbüz, E. I.; Iglesia, E. Theoretical and Kinetic Assessment of the Mechanism of Ethane Hydrogenolysis on Metal Surfaces Saturated with Chemisorbed Hydrogen. *J. Catal.* **2014**, *311*, 350−356.

(15) Katzer, J. R.; Sivasubramanian, R. Process and Catalyst Needs for Hydrodenitrogenation. *Catal. Rev.* **1979**, *20*, 155−208.

(16) Ho, T. C. Hydrodenitrogenation Catalysis. *Catal. Rev.* **1988**, *30*, 117−160.

(17) Prins, R. Catalytic Hydrodenitrogenation. *Adv. Catal.* **2001**, *46*, 399−464.

(18) Furimsky, E.; Massoth, F. E. Hydrodenitrogenation of Petroleum. *Catal. Rev.* **2005**, *47*, 297−489.

(19) Furimsky, E. Catalytic Hydrodeoxygenation. *Appl. Catal., A* **2000**, *199*, 147−190.

(20) Choudhary, T. V.; Phillips, C. B. Renewable Fuels via Catalytic Hydrodeoxygenation. *Appl. Catal., A* **2011**, *397*, 1−12.

(21) Gutierrez, A.; Kaila, R. K.; Honkela, M. L.; Slioor, R.; Krause, A. O. I. Hydrodeoxygenation of Guaiacol on Noble Metal Catalysts. *Catal. Today* **2009**, *147*, 239−246.

(22) Witzke, M. E.; Almithn, A.; Coonrod, C. L.; Hibbitts, D. D.; Flaherty, D. W. Mechanisms and Active Sites for C−O Bond Rupture Within 2-Methyltetrahydrofuran over Ni, $Ni_{12}P_5$, and $Ni_2P$ Catalysts. *ACS Catal.* **2018**, *8*, 7141−7157.

(23) Witzke, M. E.; Almithn, A.; Coonrod, C. L.; Triezenberg, M. D.; Hibbitts, D. D.; Flaherty, D. W. In Situ Methods for Identifying Reactive Surface Intermediates During Hydrogenolysis Reactions: C-O Bond Cleavage on Nanoparticles of Nickel and Nickel Phosphides. *J. Am. Chem. Soc.* **2019**, *141*, 16671−16684.

(24) Grange, P. Catalytic Hydrodesulfurization. *Catal. Rev.* **1980**, *21*, 135−181.

(25) Pecoraro, T. Hydrodesulfurization Catalysis by Transition Metal Sulfides. *J. Catal.* **1981**, *67*, 430−445.

(26) Sawhill, S. Thiophene Hydrodesulfurization over Supported Nickel Phosphide Catalysts. *J. Catal.* **2003**, *215*, 208−219.

(27) Wang, H.; Iglesia, E. Mechanism and Site Requirements of Thiophene Hydrodesulfurization Catalyzed by Supported Pt Clusters. *ChemCatChem* **2011**, *3*, 1166−1175.

(28) Almithn, A.; Hibbitts, D. Effects of Catalyst Model and High Adsorbate Coverages in Ab Initio Studies of Alkane Hydrogenolysis. *ACS Catal.* **2018**, *8*, 6375−6387.

(29) Almithn, A.; Hibbitts, D. Comparing Rate and Mechanism of Ethane Hydrogenolysis on Transition-Metal Catalysts. *J. Phys. Chem. C* **2019**, *123*, 5421−5432.

(30) Gürbüz, E. I.; Hibbitts, D. D.; Iglesia, E. Kinetic and Mechanistic Assessment of Alkanol/alkanal Decarbonylation and Deoxygenation Pathways on Metal Catalysts. *J. Am. Chem. Soc.* **2015**, *137*, 11984−11995.

(31) Meitzner, G.; Mykytka, W. J.; Sinfelt, J. H. Metal-catalyzed Reactions of Methylamine in the Presence of Hydrogen. *J. Catal.* **1986**, *98*, 513−521.

(32) Meitzner, G.; Mykytka, W. J.; Sinfelt, J. H. Kinetics of Hydrogenolysis of Methylamine on a Rhodium Catalyst. *Catal. Lett.* **1995**, *32*, 335−344.

(33) Meitzner, G.; Mykytka, W. J.; Sinfelt, J. H. Methylamine Hydrogenolysis on a Rhodium Catalyst: Kinetics at High Hydrogen Partial Pressures. *Catal. Lett.* **1996**, *37*, 137−141.

(34) Kemball, C.; Moss, R. L. The Catalytic Fission of the Carbon-nitrogen Bond I. The Reactions of Methylamine and Hydrogen on Evaporated Metal Films. *Proc. R. Soc. London, Ser. A* **1956**, *238*, 107−116.

(35) Chia, M.; Pagán-Torres, Y. J.; Hibbitts, D.; Tan, Q.; Pham, H. N.; Datye, A. K.; Neurock, M.; Davis, R. J.; Dumesic, J. A. Selective Hydrogenolysis of Polyols and Cyclic Ethers over Bifunctional Surface Sites on Rhodium-rhenium Catalysts. *J. Am. Chem. Soc.* **2011**, *133*, 12675−12689.

(36) Alcala, R. DFT Studies for Cleavage of C-C and C-O Bonds in Surface Species Derived from Ethanol on Pt(111). *J. Catal.* **2003**, *218*, 178−190.
(37) Sergeev, A. G.; Hartwig, J. F. Selective, Nickel-catalyzed Hydrogenolysis of Aryl Ethers. *Science* **2011**, *332*, 439−443.
(38) Mavrikakis, M.; Barteau, M. A. Oxygenate Reaction Pathways on Transition Metal Surfaces. *J. Mol. Catal. A: Chem.* **1998**, *131*, 135−147.
(39) Wiegand, B. C.; Friend, C. M. Model Studies of the Desulfurization Reactions on Metal Surfaces and in Organometallic Complexes. *Chem. Rev.* **1992**, *92*, 491−504.
(40) Zhu, H.; Guo, W.; Li, M.; Zhao, L.; Li, S.; Li, Y.; Lu, X.; Shan, H. Density Functional Theory Study of the Adsorption and Desulfurization of Thiophene and Its Hydrogenated Derivatives on Pt(111): Implication for the Mechanism of Hydrodesulfurization over Noble Metal Catalysts. *ACS Catal.* **2011**, *1*, 1498−1510.
(41) Wang, H.; Iglesia, E. Thiophene Hydrodesulfurization Catalysis on Supported Ru Clusters: Mechanism and Site Requirements for Hydrogenation and Desulfurization Pathways. *J. Catal.* **2010**, *273*, 245−256.
(42) Rufael, T. S.; Prasad, J.; Fischer, D. A.; Gland, J. L. Hydrogenolysis of Adsorbed Methylthiolate on the Pt(111) Surface. *Surf. Sci.* **1992**, *278*, 41−50.
(43) Todorova, T.; Prins, R.; Weber, T. A Density Functional Theory Study of the Hydrogenolysis Reaction of CH3SH to CH4 on the Catalytically Active (100) Edge of 2H-MoS2. *J. Catal.* **2005**, *236*, 190−204.
(44) Zhu, H.; Guo, W.; Jiang, R.; Zhao, L.; Lu, X.; Li, M.; Fu, D.; Shan, H. Decomposition of Methanthiol on Pt(111): a Density Functional Investigation. *Langmuir* **2010**, *26*, 12017−12025.
(45) Xu, L.; Stangland, E. E.; Mavrikakis, M. A DFT Study of Chlorine Coverage over Late Transition Metals and Its Implication on 1,2-dichloroethane Hydrodechlorination. *Catal. Sci. Technol.* **2018**, *8*, 1555−1563.
(46) Chen, N.; Rioux, R. M.; Barbosa, L. A. M. M.; Ribeiro, F. H. Kinetic and Theoretical Study of the Hydrodechlorination of CH(4-x)Cl(x) (x = 1−4) Compounds on Palladium. *Langmuir* **2010**, *26*, 16615−16624.
(47) Keane, M. A.; Park, C.; Menini, C. Structure Sensitivity in the Hydrodechlorination of Chlorobenzene Over Supported Nickel. *Catal. Lett.* **2003**, *88*, 89−94.
(48) Chary, K. V. R.; Rao, P. V. R.; Vishwanathan, V. Synthesis and High Performance of Ceria Supported Nickel Catalysts for Hydrodechlorination Reaction. *Catal. Commun.* **2006**, *7*, 974−978.
(49) Kresse, G.; Furthmüller, J. Efficiency of Ab-initio Total Energy Calculations for Metals and Semiconductors Using a Plane-wave Basis Set. *Comput. Mater. Sci.* **1996**, *6*, 15−50.
(50) Kresse, G.; Furthmüller, J. Efficient Iterative Schemes for Ab Initio Total-energy Calculations Using a Plane-wave Basis Set. *Phys. Rev. B* **1996**, *54*, 11169−11186.
(51) Kresse, G.; Hafner, J. *Ab Initio* Molecular Dynamics for Liquid Metals. *Phys. Rev. B* **1993**, *47*, 558−561.
(52) Kresse, G.; Hafner, J. Ab Initio Molecular-dynamics Simulation of the Liquid-metal-amorphous-semiconductor Transition in Germanium. *Phys. Rev. B* **1994**, *49*, 14251−14269.
(53) Kravchenko, P.; Plaisance, C.; Hibbitts, D. *A New Computational Interface for Catalysis. ChemRxiv*, 2019, DOI: 10.26434/chemrxiv.8040737.v4.
(54) Blöchl, P. E. Projector Augmented-wave Method. *Phys. Rev. B* **1994**, *50*, 17953−17979.
(55) Kresse, G.; Joubert, D. From Ultrasoft Pseudopotentials to the Projector Augmented-wave Method. *Phys. Rev. B* **1999**, *59*, 1758−1775.
(56) Hammer, B.; Hansen, L. B.; Nørskov, J. K. Improved Adsorption Energetics Within Density-functional Theory Using Revised Perdew-Burke-Ernzerhof Functionals. *Phys. Rev. B* **1999**, *59*, 7413−7421.
(57) Perdew, J. P.; Burke, K.; Ernzerhof, M. Generalized Gradient Approximation Made Simple. *Phys. Rev. Lett.* **1996**, *77*, 3865−3868.
(58) Zhang, Y.; Yang, W. Comment on "Generalized Gradient Approximation Made Simple". *Phys. Rev. Lett.* **1998**, *80*, 890.
(59) Monkhorst, H. J.; Pack, J. D. Special Points for Brillouin-zone Integrations. *Phys. Rev. B* **1976**, *13*, 5188−5192.
(60) Pack, J. D.; Monkhorst, H. J. Special Points for Brillouin-zone Integrations—a Reply. *Phys. Rev. B* **1977**, *16*, 1748−1749.
(61) Henkelman, G.; Jónsson, H. Improved Tangent Estimate in the Nudged Elastic Band Method for Finding Minimum Energy Paths and Saddle Points. *J. Chem. Phys.* **2000**, *113*, 9978−9985.
(62) Jónsson, H.; Mills, G.; Jacobsen, K. W. Nudged Elastic Band Method for Finding Minimum Energy Paths of Transitions. In *Classical and Quantum Dynamics in Condensed Phase Simulations*; Berne, B. J.; Ciccotti, G.; Coker, D. F., Eds.; World Scientific, 1998; pp 385−404.
(63) Henkelman, G.; Jónsson, H. A Dimer Method for Finding Saddle Points on High Dimensional Potential Surfaces Using Only First Derivatives. *J. Chem. Phys.* **1999**, *111*, 7010−7022.
(64) Mcvicker, G.; Baker, R. K.; Garten, R. L.; Kugler, E. L. Chemisorption Properties of Iridium on Alumina Catalysts. *J. Catal.* **1980**, *65*, 207−220.
(65) Kip, B. Determination of Metal Particle Size of Highly Dispersed Rh, Ir, and Pt Catalysts by Hydrogen Chemisorption and EXAFS. *J. Catal.* **1987**, *105*, 26−38.
(66) Almithn, A. S.; Hibbitts, D. D. Supra-monolayer Coverages on Small Metal Clusters and Their Effects on $H_2$ Chemisorption Particle Size Estimates. *AIChE J.* **2018**, *64*, 3109−3120.
(67) Au, C.-T.; Ng, C.-F.; Liao, M.-S. Methane Dissociation and Syngas Formation on Ru, Os, Rh, Ir, Pd, Pt, Cu, Ag, and Au: A Theoretical Study. *J. Catal.* **1999**, *185*, 12−22.
(68) Vojvodic, A.; Nørskov, J. K.; Abild-Pedersen, F. Electronic Structure Effects in Transition Metal Surface Chemistry. *Top. Catal.* **2014**, *57*, 25−32.
(69) Jentz, D.; Mills, P.; Celio, H.; Trenary, M. The Surface Chemistry of CN and H on Pt(111). *Surf. Sci.* **1996**, *368*, 354−360.
(70) Honkala, K.; Hellman, A.; Remediakis, I. N.; Logadottir, A.; Carlsson, A.; Dahl, S.; Christensen, C. H.; Nørskov, J. K. Ammonia Synthesis from First-principles Calculations. *Science* **2005**, *307*, 555−558.
(71) Jacobsen, C. J.; Dahl, S.; Clausen, B. S.; Bahn, S.; Logadottir, A.; Nørskov, J. K. Catalyst Design by Interpolation in the Periodic Table: Bimetallic Ammonia Synthesis Catalysts. *J. Am. Chem. Soc.* **2001**, *123*, 8404−8405.
(72) Logadottir, A.; Rod, T. H.; Nørskov, J. K.; Hammer, B.; Dahl, S.; Jacobsen, C. J. H. The Brønsted−Evans−Polanyi Relation and the Volcano Plot for Ammonia Synthesis over Transition Metal Catalysts. *J. Catal.* **2001**, *197*, 229−231.
(73) Lin, T. H.; Huang, T. P.; Liu, Y. L.; Yeh, C. C.; Lai, Y. H.; Hung, W. H. Adsorption and Reaction of Methanethiol on Pt(111). *Surf. Sci.* **2005**, *578*, 27−34.
(74) Lin, T. H.; Huang, T. P.; Liu, Y. L.; Yeh, C. C.; Lai, Y. H.; Hung, W. H. Adsorption and Thermal Reactions of Alkanethiols on Pt(111): Dependence on the Length of the Alkyl Chain. *J. Phys. Chem. B* **2005**, *109*, 14079−14084.
(75) Castro, M. E.; White, J. M. Decomposition of Methanethiol on Ni(111): a TPD and SSIMS Study. *Surf. Sci.* **1991**, *257*, 22−32.
(76) Roberts, J. T.; Friend, C. M. Reactions of Ethanethiol on Molybdenum(110): Formation and Decomposition of a Surface Alkyl Thiolate. *J. Phys. Chem. A.* **1988**, *92*, 5205−5213.
(77) Roberts, J. T.; Friend, C. M. Model Hydrodesulfurization Reactions: Saturated Tetrahydrothiophene and 1-butanethiol on Molybdenum(110). *J. Am. Chem. Soc.* **1986**, *108*, 7204−7210.
(78) Śrębowata, A.; Lisowski, W.; Sobczak, J. W.; Karpiński, Z. Hydrogen-assisted Dechlorination of 1,2-dichloroethane on Active Carbon Supported Palladium−copper Catalysts. *Catal. Today* **2011**, *175*, 576−584.
(79) Evans, M. G.; Polanyi, M. Inertia and Driving Force of Chemical Reactions. *Trans. Faraday Soc.* **1938**, *34*, 11.
(80) Bronsted, J. N. Acid and Basic Catalysis. *Chem. Rev.* **1928**, *5*, 231−338.


https://dx.doi.org/10.1021/acscatal.0c00481
*ACS Catal.* 2020, 10, 5086−5100

(81) Bell, R. P. The Theory of Reactions Involving Proton Transfers. *Proc. R. Soc. A* **1936**, *154*, 414−429.
(82) Bligaard, T.; Nørskov, J. K.; Dahl, S.; Matthiesen, J.; Christensen, C. H.; Sehested, J. The Brønsted−Evans−Polanyi Relation and the Volcano Curve in Heterogeneous Catalysis. *J. Catal.* **2004**, *224*, 206−217.
(83) Medford, A. J.; Vojvodic, A.; Hummelshøj, J. S.; Voss, J.; Abild-Pedersen, F.; Studt, F.; Bligaard, T.; Nilsson, A.; Nørskov, J. K. From the Sabatier Principle to a Predictive Theory of Transition-metal Heterogeneous Catalysis. *J. Catal.* **2015**, *328*, 36−42.
(84) Hammer, B.; Norskov, J. K. Why Gold Is the Noblest of All the Metals. *Nature* **1995**, *376*, 238−240.
(85) Pettersson, L. G. M.; Nilsson, A. A Molecular Perspective on the d-Band Model: Synergy Between Experiment and Theory. *Top. Catal.* **2014**, *57*, 2−13.
(86) Abild-Pedersen, F.; Greeley, J.; Studt, F.; Rossmeisl, J.; Munter, T. R.; Moses, P. G.; Skúlason, E.; Bligaard, T.; Nørskov, J. K. Scaling Properties of Adsorption Energies for Hydrogen-containing Molecules on Transition-metal Surfaces. *Phys. Rev. Lett.* **2007**, *99*, No. 016105.
(87) Fernández, E. M.; Moses, P. G.; Toftelund, A.; Hansen, H. A.; Martínez, J. I.; Abild-Pedersen, F.; Kleis, J.; Hinnemann, B.; Rossmeisl, J.; Bligaard, T.; Nørskov, J. K. Scaling Relationships for Adsorption Energies on Transition Metal Oxide, Sulfide, and Nitride Surfaces. *Angew. Chem., Int. Ed.* **2008**, *47*, 4683−4686.
(88) Salciccioli, M.; Chen, Y.; Vlachos, D. G. Density Functional Theory-Derived Group Additivity and Linear Scaling Methods for Prediction of Oxygenate Stability on Metal Catalysts: Adsorption of Open-Ring Alcohol and Polyol Dehydrogenation Intermediates on Pt-Based Metals. *J. Phys. Chem. C* **2010**, *114*, 20155−20166.
(89) Jones, G.; Studt, F.; Abild-Pedersen, F.; Nørskov, J. K.; Bligaard, T. Scaling Relationships for Adsorption Energies of C2 Hydrocarbons on Transition Metal Surfaces. *Chem. Eng. Sci.* **2011**, *66*, 6318−6323.
(90) Sutton, J. E.; Vlachos, D. G. Error Estimates in Semi-empirical Estimation Methods of Surface Reactions. *J. Catal.* **2013**, *297*, 202−216.
(91) Sutton, J. E.; Vlachos, D. G. Effect of Errors in Linear Scaling Relations and Brønsted−Evans−Polanyi Relations on Activity and Selectivity Maps. *J. Catal.* **2016**, *338*, 273−283.
(92) Wang, S.; Vorotnikov, V.; Sutton, J. E.; Vlachos, D. G. Brønsted−evans−polanyi and Transition State Scaling Relations of Furan Derivatives on Pd(111) and Their Relation to Those of Small Molecules. *ACS Catal* **2014**, *4*, 604−612.
(93) Bukowski, B. C.; Greeley, J. Scaling Relationships for Molecular Adsorption and Dissociation in Lewis Acid Zeolites. *J. Phys. Chem. C* **2016**, *120*, 6714−6722.


https://dx.doi.org/10.1021/acscatal.0c00481
*ACS Catal.* 2020, 10, 5086−5100